J. Fluid Mech. (1992), *vol.* 244, *pp.* 493–526

A study of singularity formation in vortex-sheet motion by a spectrally accurate vortex method

By M. J. SHELLEY

Department of Mathematics, University of Chicago, Chicago, IL 60637, USA

(Received 19 December 1989 and in revised form 29 April 1992)

Moore's asymptotic analysis of vortex-sheet motion predicts that the Kelvin–Helmholtz instability leads to the formation of a weak singularity in the sheet profile at a finite time. The numerical studies of Meiron, Baker & Orszag, and of Krasny, provide only a partial validation of his analysis. In this work, the motion of periodic vortex sheets is computed using a new, spectrally accurate approximation to the Birkhoff–Rott integral. As advocated by Krasny, the catastrophic effect of round-off error is suppressed by application of a Fourier filter, which itself operates near the level of the round-off. It is found that to capture the correct asymptotic behaviour of the spectrum, the calculations must be performed in very high precision, and second-order terms must be included in the Ansatz to the spectrum. The numerical calculations proceed from the initial conditions first considered by Meiron, Baker & Orszag. For the range of amplitudes considered here, the results indicate that Moore's analysis is valid only at times well before the singularity time. Near the singularity time the form of the singularity departs away from that predicted by Moore, with the real and imaginary parts of the solutions becoming differentiated in their behaviour; the real part behaves in accordance with Moore's prediction, while the singularity in the imaginary part weakens. In addition, the form of the singularity apparently depends upon the initial amplitude of the disturbance, with the results suggesting that either Moore's analysis gives the complete form of the singularity only in the zero amplitude limit, or that the initial data considered here is not yet sufficiently small for the behaviour to be properly described by the asymptotic analysis. Convergence of the numerical solution beyond the singularity time is not observed.

1. Introduction

A vortex sheet is a surface in an inviscid and incompressible fluid across which the velocity is discontinuous; it serves as a simple model of a high-Reynolds-number shear layer. Ideally, vortex-sheet motion could be used as the first term of the outer solution in a matched asymptotic expansions approach to studying high-Reynolds-number shear flows. Since the global existence and smoothness of a two-dimensional shear flow evolving from smooth initial conditions is guaranteed (McGrath 1967), a necessary condition for the success of such a program would be the global existence of this outer solution. However, there is now strong evidence that the two-dimensional vortex sheet acquires a singularity at a finite time well before the appearance of the large-scale roll-up commonly associated with shear layers. The possible nature and existence of vortex-sheet motion beyond the singularity time is an open question.

The first analytical evidence of singularity formation was provided by Moore

(1979, 1985). For a sinusoidally perturbed sheet with uniform strength, Moore performed a small-amplitude perturbation analysis of the Birkhoff equation, which governs vortex-sheet motion. His analysis indicated that at a finite time the curvature of the sheet profile diverged, with the sheet strength remaining finite, but acquiring a cusp. More specifically, his approximate analysis indicated the presence of a pair of branch singularities of order $\frac{3}{2}$, above and below the real axis in the extended Lagrangian variable plane, which moved to the real axis in a finite time. For specially chosen entire initial data, Meiron, Baker & Orszag (1982) (hereinafter referred to as MBO) found consistent results by studying the Taylor series in time constructed numerically from the Birkhoff equation. Using the point-vortex approximation and a Fourier filter to control the errors induced by round-off error, Krasny (1986*a*) (hereinafter referred to as Kr) studied direct simulations of vortex-sheet motion from an unstable, linear eigenfunction initial condition, and also found results consistent with Moore (1979). Moreover, before the singularity time, the numerical solution converged, but convergence was lost beyond the singularity time. While neither of these studies was able to convincingly identify the order of the branch, they both presented numerical evidence that its order was between 1 and 2. Caflisch & Orellana (1989) have found a continuum of explicit solutions to the Birkhoff equation which display finite time singularities. However, these solutions have initial data which are not entire, but which begin with branch singularities in the extended Lagrangian variable plane. The order of the branch singularity is a free parameter, and the mechanism by which a singularity is chosen by the general initial-value problem is not known. None of these studies indicate whether the sheet still exists beyond its singularity time. Other results concerning existence and well-posedness of vortex-sheet motion can be found in Sulem *et al.* (1981), Caflisch & Orellana (1986) and Caflisch & Orellana (1989).

A precise understanding of singularity formation in vortex-sheet motions is important for several reasons. First, vortex sheets are often used in models of fluid motions, and it is important to understand the limits of their applicability. For example, vortex sheets have been used successfully in the study of large-amplitude surface waves (see, for example, Longuett-Higgins & Cokelet 1976; Baker, Meiron & Orszag 1982), and in the Rayleigh–Taylor instability for a fluid falling into vacuum (Baker, Meiron & Orszag 1980; Baker *et al.* 1987). These all correspond to interfacial flows with an Attwood ratio of 1 or -1. Conversely, researchers have had considerable difficulty in simulating the Rayleigh–Taylor instability in fluids with non-unit Attwood ratio (e.g. Baker *et al.* 1980). It is believed that these difficulties are related to the formation of singularities in the vortex sheets modelling the interface between the two fluids of different densities. Secondly, Krasny (1986*b*) and Baker & Shelley (1990) have raised the intriguing possibility that the vortex sheet may exist after its singularity time as a doubly-branch spiral. Clearly then, a detailed knowledge of the formation of the singularity is crucial in deducing the form of the spiral, or if it is even an allowable possibility. Lastly, the mathematical analysis of the vortex sheet singularity is greatly simplified by knowing that it actually does have the form suggested by Moore (Caflisch, private communication).

It is known that measured-valued solutions exist globally for vortex-sheet initial data (Diperna & Majda 1987), but the notion of such a solution is so general that it gives little information about its specific nature. It is also possible that vortex-sheet motion still exists beyond its singularity time as a classical weak solution to the Euler equations, though perhaps it is no longer described by the Birkhoff–Rott equation. Consistent discretizations to the Birkhoff equation have failed to yield reliable

results beyond the singularity time, so alternative methods have been employed. Krasny (1986*b*) modified the Birkhoff equation by smoothing the singular Biot–Savart kernel through convolution with an approximate delta-function of width δ. Past the singularity time for the vortex sheet, and for a fixed value of δ, solutions to the smoothed equation reveal a doubly branched spiral structure, with the number of turns of the spiral increasing, apparently without limit, as δ is reduced.

In Baker & Shelley (1990), the vortex sheet is replaced by constant and finite vorticity contained within a thin layer of mean width H. The limiting behaviour of such vortex layers is then studied numerically, as H is reduced, to determine the possible nature of the vortex sheet past its singularity time. Beyond the singularity time, for each value of H, the vortex layer forms an elliptical core with attached, trailing arms. In the region of the boundary where the arms attach to the cores, the curvature shows very rapid growth. A natural conjecture then is that the curvature on the boundary of the layer diverges, and that these curvature singularities collapse to the vortex-sheet singularity in the limit. However, a careful examination of the computed Fourier spectrum suggests that this is not the case, and that the boundaries of the layer remain smooth. Instead, it seems the singularity forms only in the limit of zero H, as a consequence of accumulations of vorticity in the centre region. It is this accumulation for a finite value of H, which engenders the appearance of the elliptical core, with attached, trailing arms. As H is reduced at a fixed time past the singularity time, the approximation to the vortex-sheet strength associated with the core width appears to increase without bound. However, the total vortex-sheet strength associated with the core, or equivalently, the core circulation, appears to go to zero as H is reduced. Such behaviour does not preclude the existence of a classical weak solution in the zero H limit (Diperna & Majda 1987). Concomitant with this, the arms attached to the core converge away from the core, but become increasingly tightly wound in the core region.

Using a new, spectrally accurate approximation to the Birkhoff–Rott integral, singularity formation in vortex-sheet motion is re-examined, with the intent of acquiring more precise information on the singularity structure. In their study of the numerical solution of integral equations for conformal mapping, Sidi & Israeli (1988) noted that an alternate point, trapezoidal quadrature of integrals with singular, periodic Cauchy kernels, such as the integral in the Birkhoff–Rott equation, yielded spectral accuracy (i.e. is of infinite order). Unlike other quadrature rules (see, for example, Conte 1979), no singularity subtraction is performed, nor do derivative approximations need to be computed. This result is applied to the Birkhoff–Rott integral to yield an approximating set of ODEs to the Birkhoff–Rott equation, whose spatial consistency error is of infinite order. The infinite order of the quadrature follows from the fact that the asymptotic error expansion of the point-vortex approximation, as used by Rosenhead (1931), Kr and many others, has in this context only one term of algebraic order, namely $O(h)$, with the remainder being of infinite order. A simple Richardson extrapolation removes this first-order error term, yielding the spectrally accurate quadrature rule. We refer to this new semi-discrete system as the modified point-vortex approximation. As it arises as a linear combinations of point-vortex approximations to the Birkhoff–Rott integral, the modified point-vortex approximation inherits a Hamiltonian structure, and conserves the same quantities as the point-vortex approximation (i.e. circulation and moments of vorticity).

Owing to the ill-posedness of the linearized motion (the disturbance growth rate scales linearly with its wavenumber), care must be taken to control the effect of

round-off-error. To this end, we employ the Fourier filter advocated in Kr, which, at each timestep, zeros any Fourier modes with amplitude less than some given tolerance. The filter operates near the level of the machine round-off. The calculations presented here were performed in 30 digits of precision, with the filter tolerance set to 10^{-25}. It will be seen that this level of precision and filter are necessary to discern the asymptotic behaviour of the Fourier spectrum, which in turn reveals the structure of the nascent singularity.

The evolution of the vortex sheet from initial conditions first considered by MBO is studied in detail for several initial amplitudes. In addition to their numerical study, MBO also performed Moore's analysis for their initial condition, and found results identical to Moore's. Strictly speaking, Moore's analysis should be valid only for data of sufficiently small initial amplitude, at times well away from the critical time. An important question is whether it also well describes the singularity that actually forms on the sheet, and if so, whether it is generic, describing well singularity formation even in large-amplitude data. We find that for the initial conditions considered here, Moore's analysis does appear to be valid at times well before the singularity time. However, near the singularity time a transition in behaviour takes place. The real and imaginary parts of the solution become differentiated in their behaviour, with the imaginary part becoming smoother than the real part, which is itself well-described by Moore's analysis. We also find that the apparent form of the singularity depends upon the amplitude of the initial data. The results suggest that either Moore's analysis gives the full form of the singularity only in the zero-amplitude limit, or that the data considered here is not yet sufficiently small for the behaviour to be properly described by his asymptotic analysis.

Section 2 provides further background of the problem. Section 3 discusses the modified point-vortex approximation, its properties, and its relationship with other approximations. Section 4 gives the results of a numerical study of vortex-sheet evolution using the modified point-vortex approximation. This includes a detailed study of the spectrum, which reveals the form of the nascent singularity, and also a study of the straining flows about the point of singularity. Section 5 gives concluding remarks.

2. Background of the problem

The geometry of a planar vortex sheet is illustrated in figure 1. The sheet position is parametrized by a real variable p as $z(p,t) = x(p,t) + \mathrm{i}y(p,t)$, $-\infty < p < +\infty$. The variable p is chosen to be constant along paths moving with the average of the velocities on either side of the sheet, and p is now referred to as the Lagrangian variable. This yields the Birkhoff–Rott equation of vortex-sheet motion,

$$\frac{\partial z^*}{\partial t}(p,t) = \frac{1}{2\pi\mathrm{i}} P \int_{-\infty}^{+\infty} \frac{\gamma(q)}{z(p,t) - z(q,t)} \mathrm{d}q. \tag{2.1}$$

Here γ is called the vortex-sheet strength, z^* denotes the complex conjugate of z, and the Birkhoff–Rott integral is of principal value type. That γ does not depend upon time expresses the fact that the circulation is conserved along Lagrangian particle paths. The jump in tangential velocity across the interface is called the true vortex-sheet strength, and is given by

$$\hat{\gamma}(p,t) = \frac{\gamma(p)}{|z_p(p,t)|}, \tag{2.2}$$

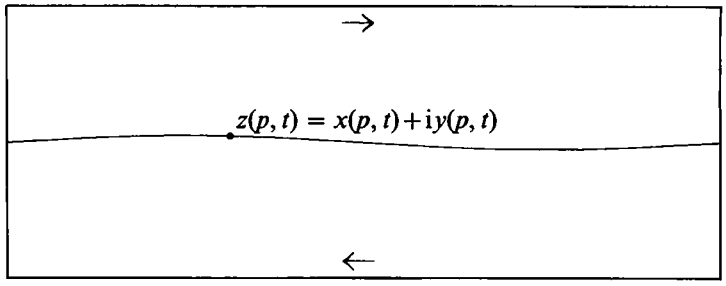

FIGURE 1. A schematic of two-dimensional, planar vortex-sheet geometry.

where the subscript p refers to partial differentiation. If the sheet initial data is 2π periodic in the x-direction, that is $z(p+2\pi, t=0) = 2\pi + z(p, t=0)$, and $\gamma(p+2\pi) = \gamma(p)$, then the subsequent motion will be also, and is governed by the periodic form of (2.1),

$$\frac{\partial z^*}{\partial t}(p,t) = \frac{1}{4\pi \mathrm{i}} P \int_0^{2\pi} \gamma(q) \cot \tfrac{1}{2}[z(p,t) - z(q,t)] \, \mathrm{d}q. \tag{2.3}$$

It is the periodic form of the Birkhoff–Rott equation that will be considered in this study. As for smooth vorticity distributions, there are constants of the motion associated with vortex-sheet motion. These include the total circulation and the first moments of the vorticity in a periodic strip, and the energy,

$$E = \int_0^{2\pi} \mathrm{d}p \, \gamma(p) \int_0^{2\pi} \mathrm{d}q \, \gamma(q) \ln \{\cosh [y(p) - y(q)] - \cos [x(p) - x(q)]\}. \tag{2.4}$$

There will sometimes be analogous constants of the motion for the discrete systems arising as approximations to vortex-sheet motion.

The chief difficulty, which makes both the analytical and numerical treatment of the Birkhoff–Rott equation very delicate, is the ill-posedness of its linearized motion, as a consequence of the Kelvin–Helmholtz instability. A simple equilibrium is given by a flat sheet with uniform sheet strength. Letting $\gamma(p) = 1 + \epsilon\tilde{\gamma}(p)$, and $z(p,t) = p + \epsilon\mu(p,t)$ with $\epsilon \ll 1$, the linearized Birkhoff–Rott equation is given by

$$\begin{aligned} \frac{\partial \mu^*}{\partial t}(p,t) &= \frac{1}{4\pi \mathrm{i}} P \int_0^{2\pi} [\tilde{\gamma}(q) - \mu_q(q,t)] \cot \tfrac{1}{2}(p-q) \, \mathrm{d}q \\ &= \tfrac{1}{2}\mathrm{i} H(\mu_q - \tilde{\gamma})(p,t), \end{aligned} \tag{2.5}$$

where H denotes the Hilbert transform (Carrier, Krook & Pearson 1966, p. 417). Letting $\tilde{\gamma}(p) = \beta_k^c \cos kp + \beta_k^s \sin kp$, (2.5) has trigonometric solutions of the form

$$\mu(p,t) = \left[\alpha_k^c \left(1 - \mathrm{i}\frac{\sigma}{|\sigma|}\right) \mathrm{e}^{\sigma t} - \frac{1}{|\sigma|}\beta_k^s\right] \cos kp + \left[\alpha_k^s \left(1 - \mathrm{i}\frac{\sigma}{|\sigma|}\right) \mathrm{e}^{\sigma t} + \frac{1}{|\sigma|}\beta_k^c\right] \sin kp, \tag{2.6}$$

where

$$\sigma^2(k) = \tfrac{1}{4}k^2. \tag{2.7}$$

Thus, there is a positive growth rate $\sigma(k) = \frac{1}{2}k$, with the linearized modes having arbitrarily large growth rates, implying an ill-posed linear motion. This is known as the Kelvin–Helmholtz instability. Birkhoff & Fisher (1959) conjectured that for the full nonlinear motion, the linear ill-posedness would cause initial data analytic in its Lagrangian variable to lose is analyticity in a finite time. Birkhoff (1962) also

conjectured that such analytic initial data for (2.1) would remain analytic for at least short times. Sulem *et al.* (1981) have proved Birkhoff's conjecture (Birkhoff 1962). Caflisch & Orellana (1986) have proved long-time existence, within the class of analytic functions, for analytical initial data that is slightly perturbed from a flat sheet. Caflisch & Orellana (1989) and Ebin (1988) have proved the ill-posedness for nonlinear vortex-sheet motion in some non-analytic function spaces.

Moore (1979, 1985) has given the first analytical evidence that a vortex sheet can lose its analyticity within a finite time through the formation of a weak singularity in the sheet profile. Moore examined the evolution from the initial condition

$$z(p, t=0) = p + \mathrm{i}\epsilon \sin p, \quad \gamma(p) = 1, \tag{2.8}$$

for $\epsilon \ll 1$. This initial condition is composed of both a growing and a decaying linear mode, as given by (2.6). The interface may be represented as the Fourier series

$$z(p,t) = p + \sum_{k=-\infty}^{k=+\infty} A_k(t)\, \mathrm{e}^{\mathrm{i}kp}, \tag{2.9}$$

with $A_k = -A_{-k}$. Substitution of (2.9) into (2.1) yields an infinite system of ordinary differential equations for the evolution of $A_k(t)$, with each equation itself containing an infinite number of terms. For small ϵ, the amplitudes $A_k(t)$ can be expanded as

$$A_k(t) = \epsilon^k A_{k,0}(t) + \epsilon^{k+2} A_{k,2} + \epsilon^{k+4} A_{k,4} + \ldots, \tag{2.10}$$

and by equating powers of ϵ, it is found that evolution of $A_{k,0}(t)$ depends only upon $A_{n,0}(t)$ for $n \leqslant k$. This system, for $A_{k,0}(t)$, is then studied for large k. In an analysis presumably valid for $k \gg 1$, Moore found the asymptotic behaviour is given by

$$\epsilon^k A_{k,0}(t) \approx \frac{(1+\mathrm{i})}{t(2\pi)^{\frac{1}{2}}} k^{-\frac{5}{2}} \exp\left[k(1 + \tfrac{1}{2}t + \ln \tfrac{1}{4}\epsilon t)\right]. \tag{2.11}$$

If $t_{\mathrm{c}}(\epsilon)$ is defined by

$$1 + \tfrac{1}{2}t_{\mathrm{c}} + \ln t_{\mathrm{c}} = \ln \frac{4}{\epsilon}, \tag{2.12}$$

then for $t < t_{\mathrm{c}}(\epsilon)$, the leading-order Fourier coefficients, $\epsilon^k A_{k,0}$, decay exponentially fast. However, for $t = t_{\mathrm{c}}(\epsilon)$, this exponential decay is lost, and $\epsilon^k A_{k,0}$ decays only algebraically as $k^{-\frac{5}{2}}$. This is the crucial result of Moore's analysis; if the full evolution of the vortex sheet is well described by this leading-order behaviour, then at $t = t_{\mathrm{c}}(\epsilon)$, the analyticity of the solution is lost.

The behaviour of the Fourier coefficients can be reinterpreted in terms of the spatial behaviour of the sheet profile. The approximate summation of the Fourier series given by $\epsilon^k A_{k,0}(t)$ yields

$$z(p,t) = p + \frac{2\sqrt{3}}{3t}(1+\mathrm{i})\{[1 - \mathrm{e}^{\mathrm{i}p}\epsilon\theta(t)]^{\frac{3}{2}} - [1 - \mathrm{e}^{-\mathrm{i}p}\epsilon\theta(t)]^{\frac{3}{2}}\} + \psi, \tag{2.13}$$

where ψ contains less singular terms. As $t \to t_{\mathrm{c}}(\epsilon)^-$, we have that $\epsilon\theta(t) \to 1^-$, and the profile acquires singularities at $p = 0, \pm 2\pi, \pm 4\pi$, etc. Thus, the singularity formation can be interpreted as the approach to the real p-axis in the periodic strip, from above and below, of a pair of branch singularities of order $\frac{3}{2}$. The analyticity strip width of the solution, or the distance of the singularity pair from the real axis, is given by $\alpha(t) = \sim (1 + \frac{1}{2}t + \ln \frac{1}{4}\epsilon t)$.

MBO also examine vortex-sheet evolution, but from the initial condition

$$z(p, t=0) = p, \quad \gamma(p) = 1 + a\cos p. \tag{2.14}$$

Again, for small a this initial condition is a combination of a growing and a decaying linear mode, as given by (2.6). MBO also found evidence of an isolated singularity forming in the sheet profile at a finite time. In addition to repeating Moore's asymptotic analysis for this initial condition, they also studied the singularity formation using extended time series methods. For Moore's analysis, the expansion of the Fourier amplitudes is in a, rather than ϵ. They found that to leading order the analysis gave results for initial condition (2.14) identical to those for (2.8); the MBO results are obtained by merely substituting a for ϵ in (2.10), (2.11) and (2.12). Their study using extended time series gave results different from those predicted by Moore's analysis. The series methods indicated that at the singularity time, $|A_k(t_c)| \approx k^{-2.7\pm0.2}$, rather than $k^{-2.5}$, as given by Moore's analysis. They were unable to assign a definitive cause to the discrepancy, attributing it perhaps to higher-order corrections dropped in Moore's analysis. They also found that $t_c(a)$, as calculated from (2.12), was typically an underestimate of the singularity time.

Krasny (1986*a*) also studied vortex-sheet singularity formation, now proceeding from initial conditions that are unstable eigenfunctions for the Kelvin–Helmholtz instability. In agreement with Moore and MBO, Krasny found evidence for the appearance of a weak singularity in the sheet profile at a finite time. In particular, he studied the evolution of vortex sheets from initial conditions of the form

$$z(p, t=0) = p + (1-\mathrm{i})\,\epsilon \sin p, \quad \gamma(p) = 1. \tag{2.15}$$

In addition to performing Moore's analysis for (2.15), Kr also performed direct simulations of vortex-sheet motion using the point-vortex approximation to the Birkhoff–Rott equation, and a Fourier filtering technique to control the growth of errors introduced by the round-off of the calculation. The Fourier amplitudes, $A_k(t)$, were approximated from the numerical data using the discrete Fourier transform, and the behaviour of the approximate amplitudes was studied. Kr assumed that in some range of sufficiently large k the approximate amplitudes had the form suggested by Moore's analysis, or

$$|A_k(t)| \approx C(t)\, k^{-\beta(t)}\, \mathrm{e}^{-\alpha(t)k}. \tag{2.16}$$

Thus, if $\alpha(t)$ goes to zero at some finite time, as Moore's analysis indicates is the case, the decay of the Fourier spectrum is purely algebraic, indicating some derivative singularity whose order is determined by the value of β at this critical time. The parameters C, β, and α were estimated using a least squares fit over some range in k, and the behaviour in time of these approximated parameters is examined. This analysis suggested that $\alpha(t)$ did become zero at a finite time. However, Kr was unable to obtain reliable estimates for the value of β, which Moore's analysis indicated should be $\beta(t) = \frac{5}{2}$, independent of time. It is shown in §4 that to get such estimates, much higher precision must be used (29 digits *vs.* 15 digits), and higher-order terms must be included in (2.16).

3. The modified point-vortex approximation

In this section the numerical approximations used for calculating vortex-sheet motion are discussed. This will focus mostly on quadrature methods for the Birkhoff–Rott integral, together with the properties of these approximations. Here

will be given a new, spectrally accurate quadrature of the Birkhoff–Rott integral. This quadrature is closely related to the point-vortex approximation, and preserves many of the favourable properties of that approximation. We begin with a discussion of the point-vortex approximation.

Following Rosenhead (1931), Krasny (1986*a*) used the point-vortex approximation (subsequently referred to as the PVA) to study vortex-sheet motion. Discretizing $z(p, t = 0)$ and $\gamma(p)$ uniformly in the Lagrangian parameter p as $z_j(t = 0) = z(jh, t = 0)$ and $\gamma_j = \gamma(jh)$, with $h = 2\pi/N$ and $j = O(1)N$, (2.1) is approximated by the set of ordinary differential equations

$$\frac{\mathrm{d}}{\mathrm{d}t} z_j^*(t) = \frac{1}{4\pi \mathrm{i}} h \sum_{\substack{k=0 \\ k \neq j}}^{N-1} \gamma_k \cot \tfrac{1}{2}(z_j(t) - z_k(t)). \tag{3.1}$$

The PVA is the trapezoidal rule approximation to the periodic Birkhoff–Rott integral, omitting the singular contribution at $k = j$. This set of discrete equations is then numerically integrated, and its behaviour studied, as far as is practically possible, in the limit of large N. The spatial consistency error, or the quadrature error, of the PVA is $O(h)$. Caflisch & Lowengrub (1989) have proved that for initial data close to the flat equilibrium, the PVA converges to the motion of vortex sheet.

Presupposing the strict positively (or negativity) of $\gamma(p)$, the discrete set of equations, (3.1), forms a Hamiltonian system with Hamiltonian

$$H_N = h \sum_{j=0}^{N-1} \gamma_j h \sum_{\substack{k=0 \\ k \neq j}}^{N-1} \gamma_k \ln [\cosh (y_j - y_k) - \cos (x_j - x_k)], \tag{3.2}$$

where the conjugate variables p_m and q_m are related to the spatial variables x_m and y_m by

$$p_m = (8\pi h \gamma_m)^{\frac{1}{2}} y_m, \quad q_m = (8\pi h \gamma_m)^{\frac{1}{2}} x_m.$$

Consequently, H_N is a constant of the motion. H_N can also be related to the energy E of the vortex sheet by noting that H_N is an $O(h)$ accurate quadrature of the energy given in (2.4), with the quadrature being of a form consistent with the PVA discretization of the Birkhoff–Rott equation. In addition to the Hamiltonian, the PVA has as constants of the motion discrete analogues of the circulation and the first moments of vorticity in a periodic strip.

As with the vortex sheet, a simple equilibrium of (3.1) is given by $z_k(t) = kh$, $\gamma_k = 1$. Associated with this equilibrium is an discrete dispersion relation, analogous to (2.7), given by

$$\sigma_N^2(k) = \tfrac{1}{4} k^2 \left(1 - \frac{k}{N}\right)^2, \tag{3.3}$$

for $k = O(1)\frac{1}{2}N$ (Lamb 1932). Note that the linearized discrete system (3.1) can evince a high wavenumber growth very similar to that of the vortex sheet, and that (2.7) is recovered as $N \to \infty$ for fixed k. The largest discrete growth rate is at the highest wavenumber allowed on the mesh, $k = \frac{1}{2}N$, with growth rate $\sigma_N(k = \frac{1}{2}N) = \frac{1}{4}N$, or half the growth rate for the same wavenumber in the true sheet motion. Practically speaking, this means that perturbations from the round-off error of the calculation can (and will) lead to the rapid and spurious growth of the high-wavenumber amplitudes, causing a rapid departure of the computed solution of the discrete system from approximating the continuous system. For this reason, Kr employed a Fourier filter that, at each timestep, zeroed any Fourier amplitude whose modulus

was less than some preassigned tolerance. By choosing this tolerance to be close to the round-off error of the calculation, it should, in principle, effect mainly those modes whose amplitude is being determined by the action of round-off error, rather than the nonlinear dynamics of the motion. The utility of such a device for calculating vortex-sheet motion with finite precision is well-documented by Kr. This device is also used in this work, but in contrast to Kr, it is not found that the use of the filter is equivalent to calculating in a higher precision, and find that care must be taken to determine the effect of the filter level, and the precision which determines it, on the calculated solution.

There is another approximation to the Birkhoff–Rott equation, based upon the trapezoidal rule at alternate points, which is closely related to the PVA, does not require the approximation of any derivatives, and is yet spectrally accurate. Specifically, this quadrature rule gives

$$\frac{\mathrm{d}}{\mathrm{d}t}z_j^*(t) = \frac{(2h)}{4\pi\mathrm{i}} \sum_{\substack{k=0 \\ j+k\,\mathrm{odd}}}^{N-1} \gamma_k \cot\tfrac{1}{2}[z_j(t)-z_k(t)], \tag{3.4}$$

as an approximation to (2.1). Here N is assumed to be even. We refer to (3.4) as the modified PVA, or MPVA.

To see the connection between the PVA and the MPVA, their respective errors as approximations to the Birkhoff–Rott integral must be examined. Not only will it be seen that the PVA is of first-order accuracy, while the MPVA is of infinite order, but that the MPVA arises through one Richardson extrapolation of the PVA error expansion.

We begin by showing an upper bound on the quadrature error of the trapezoidal rule to the integral of a periodic, analytic function over its period. Let $g(p)$ be periodic on $[0, 2\pi]$, and analytic within the strip $[-\mathrm{i}\rho, +\mathrm{i}\rho]$, including its boundary, about the real p-axis with $0 < \rho < \infty$. Then

$$|\Delta_h| = \left| \int_0^{2\pi} g(p)\,\mathrm{d}p - h \sum_{k=0}^{N-1} g(kh) \right| \leqslant C(\rho) \frac{\mathrm{e}^{-\rho N}}{1-\mathrm{e}^{-\rho N}},$$

and consequently,

$$|\Delta_h| \leqslant 2C(\rho)\,\mathrm{e}^{-\rho N} \tag{3.5}$$

for sufficiently large N. This follows from expressing Δ_h as the aliasing error of the zeroth mode of the discrete Fourier transform of g_k from the zeroth mode of the Fourier transform of $g(p)$. This may then be easily bounded through an application of Cauchy's theorem. The error bound in (3.5) is a typical realization of spectral accuracy; the error decreases faster than any algebraic power of $1/N$. The Birkhoff–Rott integral will now be rewritten so that this result becomes applicable.

Without being specific, assume that $\gamma(q)$, and $z(q)$ are analytic in some strip about the real q-axis. Assume also that $z(q)$ is a single-valued function of q, and that $z_q(q) \neq 0$ for any q. All of these assumptions are justified, for at least short times in the small-amplitude regime, by the various regularity results previously given for vortex-sheet notion (Caflisch & Orellana 1986; Sulem *et al.* 1981). Without loss of generality, set $p = 0$, and assume $z(0) = 0$. Letting $f(q) = \gamma(q)\cot\frac{1}{2}z(q)$, and using the periodicity of the integrand, now consider the integral centred about the origin, or

$$I = P\int_{-\pi}^{\pi} f(q)\,\mathrm{d}q,$$

and its two approximations,

$$I_1^h = h \sum_{\substack{k=-\frac{1}{2}N \\ k\neq 0}}^{\frac{1}{2}N-1} f_k, \quad I_2^h = 2h \sum_{\substack{k=-\frac{1}{2}N \\ k\,\text{odd}}}^{\frac{1}{2}N-1} f_k.$$

Clearly, I_1^h corresponds to the PVA, and I_2^h to the MPVA. Now, let $f(q) = \mathrm{Ev}(q) + \mathrm{Od}(q)$, where $\mathrm{Ev}(q) = \frac{1}{2}[f(q)+f(-q)]$ and $\mathrm{Od}(q) = \frac{1}{2}[f(q)-f(-q)]$. Note that $\mathrm{Od}(q)$ is an odd function about the origin, and has a simple pole there. On the other hand, $\mathrm{Ev}(q)$ is analytic in a strip about the real q-axis, with a removable singularity at $q = 0$. Now using the fact that the principal value integral over $[-\pi, \pi]$ of an odd function is zero yields

$$I = \int_{\pi}^{\pi} \mathrm{Ev}(q)\,\mathrm{d}q.$$

Both the MPVA and the PVA preserve this feature, likewise yielding

$$I_1^h = h \sum_{\substack{k=-\frac{1}{2}N \\ k\neq 0}}^{\frac{1}{2}N-1} \mathrm{Ev}_k, \quad I_2^h = 2h \sum_{\substack{k=-\frac{1}{2}N \\ k\,\text{odd}}}^{\frac{1}{2}N-1} \mathrm{Ev}_k.$$

Thus the MPVA is the trapezoidal rule approximation, over alternate points, to the integral over the period of a periodic, analytic function. The spectral accuracy follows from the previous remarks. Sidi & Israeli (1988), in their study of the numerical solution of the integral equations for conformal mapping, have shown that the alternate point trapezoidal rule yields spectral accuracy for a class of integrals with singular and periodic kernels, of which the Birkhoff–Rott integral is a special case. Note that the PVA is also a trapezoidal rule approximation of the same periodic and analytic function, now over all points except $k = 0$. It is the omission of this term that yields the $O(h)$ error. The inclusion of this term leads to the approximation of Van de Vooren (1980),

$$\frac{\mathrm{d}}{\mathrm{d}t} z_j^*(t) = h \frac{1}{4\pi \mathrm{i}} \sum_{\substack{k=0 \\ k\neq j}}^{N-1} \gamma_k \cot \tfrac{1}{2}[z_j(t) - z_k(t)] + h \frac{1}{2\pi \mathrm{i}} \frac{\gamma_j z_{ppj}(t) - 2\gamma_{pj} z_{pj}(t)}{2 z_{pj}^2(t)}. \tag{3.6}$$

Here, the order of the quadrature error is determined by how accurately z_{pj} and z_{ppj} are approximated. For example, discrete Fourier transforms could be used to yield spectral accuracy.

An alternate interpretation would be to note that the only algebraic error term in the quadrature error for the PVA comes from the $k = 0$ term. A single Richardson extrapolation removes this order h term, yielding the MPVA and spectral accuracy.

Another high-order quadrature of the Birkhoff–Rott integral uses the identity

$$\frac{1}{4\pi \mathrm{i}} P \int_0^{2\pi} z_q(q) \cot \tfrac{1}{2}[z(p) - z(q)]\,\mathrm{d}q = 0.$$

Equation (2.1) is then rewritten as

$$\frac{\partial z^*}{\partial t}(p,t) = \frac{1}{4\pi \mathrm{i}} \int_0^{2\pi} \frac{\gamma(q)\, z_p(p,t) - \gamma(p)\, z_q(q,t)}{z_p(p,t)} \cot \tfrac{1}{2}(z(p,t) - z(q,t))\,\mathrm{d}q. \tag{3.7}$$

The integrand in (3.7) is now smooth and periodic, having made the singularity at $q = p$ removable. If $z(p)$ and $\gamma(p)$ are again discretized uniformly in their parametric

variable p, the trapezoidal rule may be applied to yield spectral spatial accuracy. Here $z_q(q)$ at the mesh points would be found using the discrete Fourier transform (again, spectrally accurate). The trapezoidal rule can be applied in at least two ways. One may choose to perform the quadrature over all the points, taking the appropriate limiting value at the point where $p = q$ (and for which $z_{qq}(q)$ must be approximated), or the quadrature may be performed over alternate points (see Baker & Shelley 1986), thus avoiding the evaluation of the integrand at the indeterminate point.

Finally, note that these arguments are only concerned with the spatial consistency of the MPVA, not with its convergence to the time-dependent motion of the sheet. Hou, Lowengrub & Krasny (1991) have now proved that, for initial data sufficiently close (in the appropriate sense) to the flat equilibrium, the MPVA converges with infinite order to the motion of vortex sheet. Their method of proof does not extend to times when the data is large, much less the singularity time. However, even when the analyticity strip width is zero the MPVA remains a convergent quadrature of the Birkhoff–Rott integral for a branch singularity of order $\frac{3}{2}$, such as is posited by Moore (setting $\epsilon\theta = 1$ in (2.13)). In this case, while there is no exponential convergence in N, the error can still be bounded by an algebraic error of $O(1/N^{\frac{1}{2}})$.

As the MPVA arises from the PVA through a Richardson extrapolation, it is hardly surprising that the MPVA is also a Hamiltonian system. A Hamiltonian for this system can again be found by a consistent discretization of the energy E, or

$$\hat{H}_N = h \sum_{j=0}^{N-1} \gamma_j 2h \sum_{\substack{k=0 \\ j+k \text{ odd}}}^{N-1} \gamma_k \ln\left[\cosh(y_j - y_k) - \cos(x_j - x_k)\right], \tag{3.8}$$

with the same conjugate variables as the PVA. Note that (3.8) is only an $O(h)$ approximation to E, and it would seem contradictory that a spectrally accurate approximation to the Birkhoff–Rott integral could arise from it. Fortunately, $\hat{H}_N$ differs from being a spectrally accurate approximation to E by only a time-independent term, which can be given explicitly. A Hamiltonian which is a spectrally accurate approximation to E is given by

$$H_N = \hat{H}_N + h \sum_{j=0}^{N-1} \gamma_j \left[\int_0^{2\pi} \gamma(q) \ln\left[1 - \cos(jh - q)\right] dq - 2h \sum_{\substack{k=0 \\ j+k \text{ odd}}}^{N-1} \gamma_k \ln\left[1 - \cos(jh - kh)\right] \right]. \tag{3.9}$$

The correction term is independent of the solution $x_j(t)$ and $y_j(t)$, and does not modify the equations of motion. In principle, it can be calculated to as high an accuracy as desired, as $\gamma(q)$ is assumed known. For the initial data for x and y considered in this work, the correction term can be calculated in closed form. Thus, H_N is a constant of the motion for the discrete system, and a spectrally accurate discretization of the energy E. Nonetheless, H_N is a constant of the motion associated with the semi-discrete equations, and its spectral accuracy aside, is only useful as a check of time-integration errors. In addition, we note that as with the vortex sheet and the PVA, the circulation and first moments of the vorticity in a period are constants of the motion for the MPVA.

Again, a simple equilibrium is given by $z_k(t) = kh$ and $\gamma_k = 1$. As pointed out by G. Baker, its discrete dispersion relation matches that of the continuous system exactly, or

$$\sigma_N^2(k) = \tfrac{1}{4}k^2, \tag{3.10}$$

for $k = O(1)\frac{1}{2}N$. This is a reflection of the spectral accuracy of the approximation, but is also an argument for the necessity of the Fourier filter in controlling the behaviour of the high modes in the calculation. Again, the fastest growing discrete mode is at the largest wavenumber on the mesh, $k = \frac{1}{2}N$.

4. Numerical results

The results of a numerical study of singularity formation in vortex-sheet motion are given in this section. In particular, vortex-sheet evolution from initial conditions (2.14) is studied for several values of a. As discussed in detail in §2, MBO found strong evidence for singularity formation from these initial conditions, both by using Moore's analysis, and by studying Taylor series in time that were constructed numerically. Here, using the MPVA, the vortex sheet is numerically evolved forward in time, and its behaviour is studied as the numerical parameters of the approximation are varied. A fourth-order, Adams–Moulton, predictor–corrector method is used for time integration. The numerical parameters are not only N, the number of ODEs, and the timestep Δt, but also the tolerance level δ of the Fourier filter. The minimum value of δ is dictated by the available precision of the calculation. It is both δ and N that determine the number of Fourier modes that participate in the calculation of the Birkhoff–Rott integral. Assume that the spectrum is given and that it decays monotonically, at least for sufficiently large k. That is, $|A_{k+1}(t)| < |A_k(t)|$ (and of course that $A_k(t) \to 0$ as $k \to \infty$). Then, given a $\delta > 0$ there exists a K_δ, such that $|A_k| < \delta$ for all $k > K_\delta$. All such modes are set to zero by the Fourier filter. Thus, the number of modes participating in the integral evaluation is min $(K_\delta, \frac{1}{2}N)$. The value of δ can have a large effect when attempting to discern delicate details of the decay of the spectrum. Here, the calculations are performed in 29 digit arithmetic (Cray double precision) with $\delta = 10^{-25}$. Strictly speaking, δ should be treated as a convergence parameter, with its effect upon the calculation studied as its value is reduced as far as is practically possible. For an illustrative case, both the values of δ and N are varied ($\delta = 10^{-14}$, 10^{-20}, and 10^{-25}) to discern the effect upon the approximate solution. If varying δ can be interpreted as the effect of varying precision (and numerical experiments suggest that it can) it illustrates that very high precision is necessary to uncover the correct asymptotic decay of the spectrum, at times both away and near the singularity time. Such high precision calculations are expensive, and their speed depends upon the hardware and software implementation of double precision. On the Cray-2, a velocity evaluation, using the MPVA, in double precision with $N = 512$ takes 5.5 s, versus 0.1 in single precision. Nonetheless, a resolution study is provided, which indicates that spectral convergence is maintained to very near the singularity time.

Additionally, a very different technique is used for analysing the numerically computed spectrum to those used in previous studies (Sulum, Sulem & Frisch 1983; Kr; Baker & Shelley 1989). Rather than estimating the decay of the spectrum through a least squares fit over a range of wavenumbers k, with the form given by (2.16), the spectrum is fit point-wise in k with a form which includes (2.16), but also attempts to capture higher-order effects. Pugh (1989), using a lower-order approximation to the spectrum, first employed such a point-wise fit to the spectrum in his study of Boussinesq flows.

As a result, we provide strong evidence that the Fourier series of $z(p,t) - p$ decays asymptotically as predicted by (2.11), but only at times away from the singularity time. Moore's analysis is presumably valid only for $t \ll t_c$ and sufficiently small initial

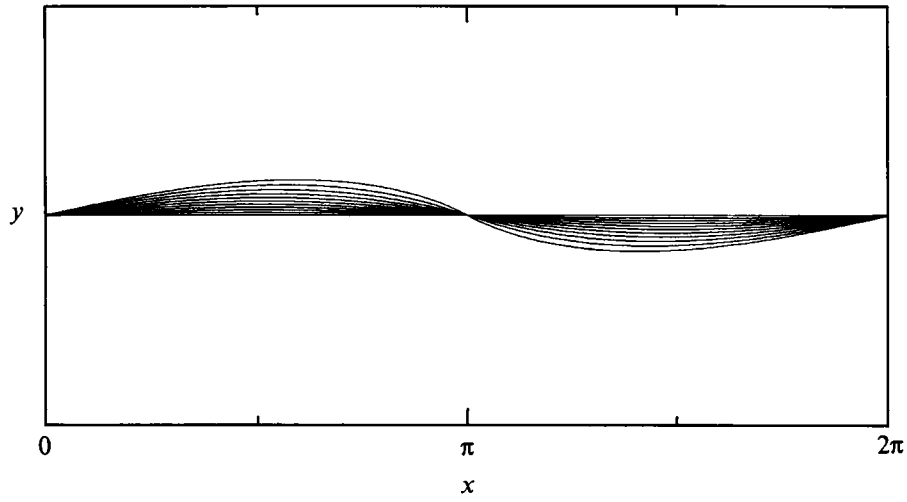

FIGURE 2. The evolution of the vortex sheet, with $a = \frac{1}{8}$, for the MBO initial conditions, from $t = 0$ to 3.0 at intervals of 0.3. $t \approx 3.015$ is the estimated singularity time.

data. It has not been known whether it generally and precisely described the singularity itself. In its main points, Moore's analysis appears to be adequate. It predicts the formation of the singularity at a finite time, that the curvature diverges at this time, and that the true vortex-sheet strength acquires a cusp. There are some disagreements. In accordance with MBO, we find that Moore's analysis, through (2.12), underpredicts the singularity time. At this predicted singularity time, the solution is still smooth (analytic), and from this time there begins a transition in the decay of the Fourier series away from that given by (2.11). This transition leads to a differentiation in behaviour of the real and imaginary parts of the solution; the real part behaves in accordance with Moore's prediction, while the singularity in the imaginary part weakens. We also find that the form of the singularity depends upon the initial amplitude, and the results may suggest that either Moore's analysis gives the form of the singularity only in the limit of zero amplitude, or that Moore's results are only realized at yet smaller values of the initial amplitude. We begin with a study of vortex-sheet evolution at times away from the singularity time.

4.1. *The validity of Moore's analysis away from the singularity time*

As has been remarked previously (Moore 1979; MBO; Kr), the singularity appears in the sheet profile well before the occurrence of any of the large-scale roll-up typically associated with the instabilities of shear layers. Using the MPVA, the vortex sheet is evolved forward from the initial conditions

$$z(p, t = 0) = p, \quad \gamma(p) = -1 + a\cos p, \tag{4.1}$$

for various values of a. This is just the initial condition (2.14), after a translation by π in p, and a change in sign of the vortex-sheet strength. This form is used for historical reasons, and the only difference in behaviour is that the singularities now occur at $p = \ldots, -\pi, \pi, \ldots$.

First, we consider our smallest-amplitude initial condition $a = 0.125$. For this value of a, (2.12) predicts that $t_c \approx 2.84$. Figure 2 shows the sheet profile from $t = 0$ to 3.0, at intervals of 0.3. The calculation used $N = 256$, $\Delta t = 0.01$, and $\delta = 10^{-25}$. This

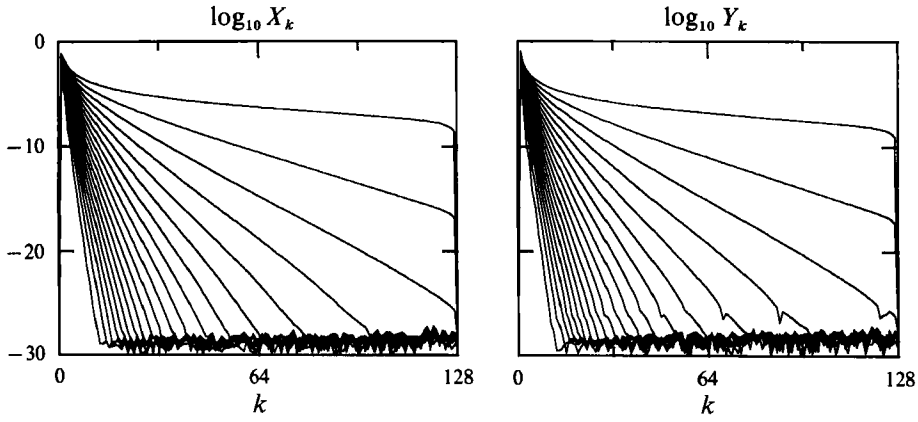

FIGURE 3. The evolution of $X_k(t)$ and $Y_k(t)$, with $a = \frac{1}{8}$, from $t = 0$ to 3.0 at intervals of 0.15.

timestep is sufficiently small so that the Hamiltonian H_N was conserved to at least 10 digits throughout the calculation. At the last time shown, $t = 3.0$, the sheet is not much perturbed from its initial condition, and still appears quite smooth. Nonetheless, the sheet is very close to its singularity time, which is estimated to be $t_c \approx 3.015$. We proceed with an analysis of the spectrum, first considering the behaviour up to $t = 2.85$.

Moore's analysis for the initial condition (4.1) gives that the Fourier amplitudes, $A_k(t)$, should behave as

$$A_k(t) \approx (-1)^k \frac{(1-\mathrm{i})}{t(2\pi)^{\frac{1}{2}}} k^{-\frac{5}{2}} \exp\left[k(1+\tfrac{1}{2}t+\ln\tfrac{1}{4}at)\right], \tag{4.2}$$

for $t \ll t_c$ and $k \gg 1$. As in Kr, this form is used as an Ansatz for the behaviour of the numerically computed spectrum, though now the behaviours of the real and imaginary parts of the solution are considered separately. Figure 3 shows the evolution of the discrete Fourier transforms, $X_k(t)$ and $Y_k(t)$, of $x_j(t)-jh$ and $y_j(t)$ from $t = 0$ to $t = 3.0$ at intervals of 0.15. As the solutions, $x(p,t)-p$ and $y(p,t)$, evolving from the MBO initial conditions can each be represented as a sine series, their Fourier transforms have a symmetry about $k = 0$, and only positive k need be considered. The most notable feature in the spectra is the very rapid temporal growth of the high-wavenumber amplitudes.

To study the behaviour of the spectrum, which presumably reveals the form of the nascent singularity, (4.2) is used as an Ansatz for it asymptotic decay. Assume that for $k \gg 1$,

$$|X_k(t)| = C_X k^{-\beta_X} \exp(-\alpha_X k), \quad |Y_k(t)| = C_Y k^{-\beta_Y} \exp(-\alpha_Y k). \tag{4.3a, b}$$

Rather than estimate, for example, the values of C_X, α_X, and β_X by a least squares fit to X_k over some range of k (as in Sulem *et al.* 1983; Kr; Baker & Shelley 1990), these values are instead estimated by requiring that the form (4.3*a*) hold point-wise at $k-1$, k and $k+1$. By taking a logarithm of both sides of (4.3*a*), this yields three linear equations for the three unknowns $\alpha_X(k)$, $\beta_X(k)$, and $C_X(k)$. As (4.3*a*) should be only asymptotic in k, the behaviours of the unknowns should be examined as $k \to \infty$. Of course, in a numerical simulation there are the added constraints of having only a finite number of amplitudes $X_k(\frac{1}{2}N)$, and having the various errors in their

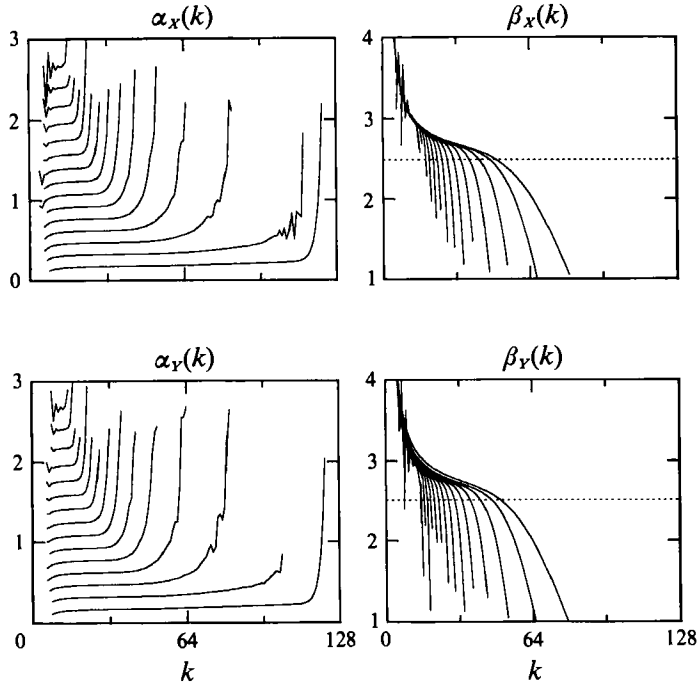

FIGURE 4. The fits to α_X, β_X, α_Y and β_Y using Ansatz (4.3), with $a = \frac{1}{8}$, from $t = 0.90$ to 2.85 at intervals of 0.15. Decreasing values in the k-independent region of α_X and α_Y corresponds to increasing time. An increasing range of upward concavity for β_X and β_Y corresponds to increasing time. The dashed line is at $\frac{5}{2}$.

approximation, such as aliasing, truncation, and round-off. Each of these sources of error limits the range in K over which the fit is expected to be accurate. However, this technique allows for a more precise study of the behaviour of the spectrum by removing some of the subjective biases present in a least squares fit (such as choosing the range in k). It will be seen presently that (4.3) is not fully adequate in deducing the behaviour of the spectrum, and will have to be modified.

Note that Moore's analysis gives the values of both β_X and β_Y to be $\frac{5}{2}$, independent of k and t, and that α_X and α_Y are equal, independent of k, and monotonically decrease as functions of t. Figure 4 shows the fits to α_X, β_X, α_Y and β_Y as functions of k, from $t = 0.90$ to 2.85 at intervals of 0.15. Note that for a large range of k, both α_X and α_Y show little dependence upon k, and that as time increases, the k independent values of α_X and α_Y tend towards zero. Also, the values of α_X and α_Y in the k independent range coincide in value. All of these features are consistent with Moore's analysis. The fits to β_X and β_Y, at first glance, are quite different from the uniform $\frac{5}{2}$ predicted by Moore's analysis. However, it appears that over some range of k, the fit to β_X and β_Y is decreasing and concave upwards. If this is the true behaviour of the fit in the absence of approximation errors, it might suggest that β_X and β_Y are asymptotic to some value. The value of $\frac{5}{2}$ has been included suggestively as a dashed line in the graphs. Recall that Moore's analysis is only asymptotic in large k, and that higher-order effects excluded in the analysis may influence the fit.

A partial inclusion of such higher-order effects is obtained by modifying the Ansatz (4.3). The real part of the solution serves as an example. Assume that $x(p)-p$ has a pair of branch singularities of the form (2.13) in its analytic continuation, but now

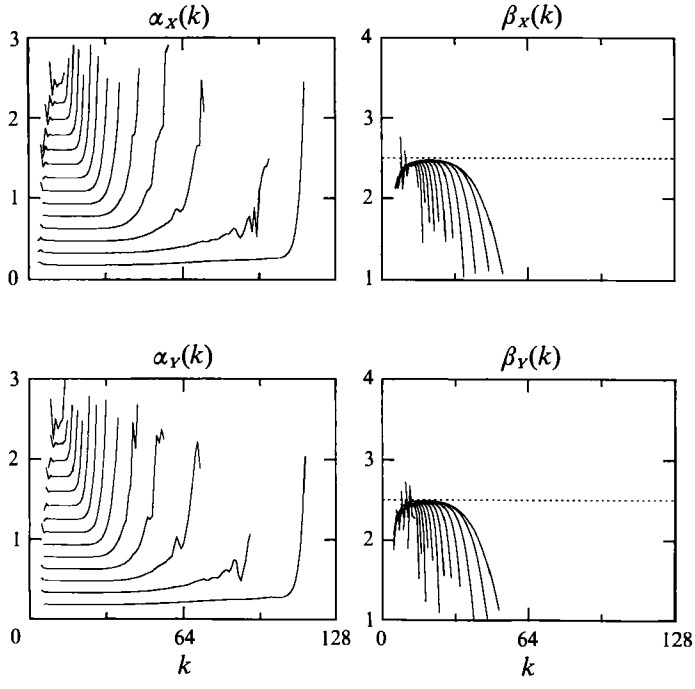

FIGURE 5. The fits to α_X, β_X, α_Y and β_Y, now using Ansatz (4.4), for $a = \frac{1}{8}$, at the same times as figure 4.

of an unspecified order $\beta_X - 1$, rather than $\frac{3}{2}$. The asymptotic decay of X_k is governed by these singularities. The first two terms of the large k expansion for X_k have the form

$$|X_k(t)| = C_X k^{-\beta_X} \exp(-\alpha_X k) + D_X k^{-(\beta_X+1)} \exp(-\alpha_X k)$$
$$= C_X k^{-\beta_X} \exp(-\alpha_X k)\left(1 + \frac{D_X}{C_X}\frac{1}{k}\right),$$

or

$$\ln|X_k(t)| = \ln C_x - \beta_X \ln k - \alpha_X k + \ln\left(1 + \frac{D_X}{C_X}\frac{1}{k}\right)$$
$$= \ln C_x - \beta_X \ln k - \alpha_X k + \frac{D_X}{C_X}\frac{1}{k} + O\left(\frac{1}{k^2}\right). \tag{4.4}$$

Here α_X is the distance of the branch singularities from the real p-axis. Dropping the $O(1/k^2)$ term, (4.4) is the new form used in the fit to the spectrum, and requires fitting to four consecutive points to yield four linear equations for the four unknowns. Figure 5 is the same as figure 4, except that Ansatz (4.4) is now used. It is clear that in the range for which β_X and β_Y were concave upwards in the old fit, they were asymptotic to $\frac{5}{2}$. The fits for α_X and α_Y from (4.4) are virtually identical to those from the old fit. Note that the estimates for β_X and β_Y using Ansatz (4.3) (i.e. only the first-order term) are asymptotic to $\frac{5}{2}$ from above. This may account for the too high estimates of the algebraic decay given by MBO. Note that $t = 2.85$ (the last time shown in figure 4) is approximately the singularity time predicted by (4.2), and that the k independent values of α_X and α_Y are well away from zero. This implies that the solution is still smooth.

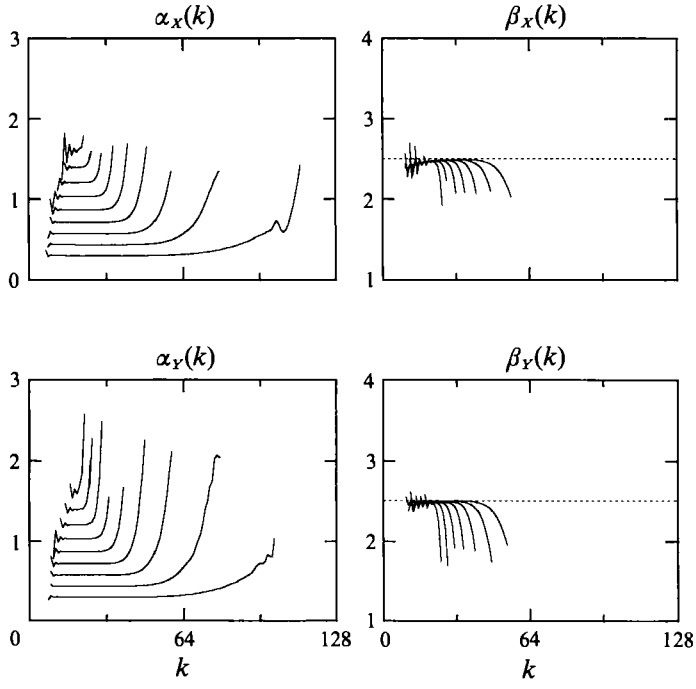

FIGURE 6. The fits to α_X, β_X, α_Y and β_Y using Ansatz (4.4), for $a = \frac{1}{2}$, from $t = 0.60$ to 1.4 at intervals of 0.1. The dashed line is at $\frac{5}{2}$.

That Moore's analysis is valid away from the singularity time appears to be independent of the amplitude of the initial condition. Figure 6 shows the fits to α_X, β_X, α_Y and β_Y, using Ansatz (4.4) for $a = 0.5$. from $t = 0.6$ to 1.4 at intervals of 0.1. Here, the calculation used $N = 256$, $\Delta t = 0.0025$, and $\delta = 10^{-25}$. This timestep is sufficiently small so that the Hamiltonian is again conserved to at least 10 digits throughout the calculation. Moore's analysis gives the estimated singularity time as $t_c \approx 1.44$. The same asymptotic behaviour of the spectrums is observed here as for the smaller-amplitude case: the algebraic part of the decay is $k^{-\frac{5}{2}}$, the k independent ranges of α_X and α_Y show a decrease in value toward zero as time increases, but with these values still non-zero at the critical time predicted by (4.2). Behaviour in accordance with Moore's analysis is also observed for $a = 0.25$ and 1.0 at times away from their respective singularity times.

It is appropriate here to examine the influence of N and δ upon the results. This has been done most completely for the case $a = 0.5$. Performing such a study for each value of a considered is beyond our resources, but it demonstrates that a high level of precision and a small value of the filter level δ are necessary to capture the correct form of the nascent singularity.

As discussed at the beginning of this section, it is both these quantities that determine the number of modes that participate in the calculation at some time. Again, assume that the spectrum is given and is monotonically decreasing as a function of k. If $\delta > 0$ is fixed, then for sufficiently large N it will be that $K_\delta = \min(K_\delta, \frac{1}{2}N)$, that is, the number of non-zero modes (and the accuracy of the approximation) is determined mainly by the value of δ, not by the value of N. This result is very much realized in these calculations, and has a marked effect on the ability to deduce delicate information about the singularity formation, as revealed

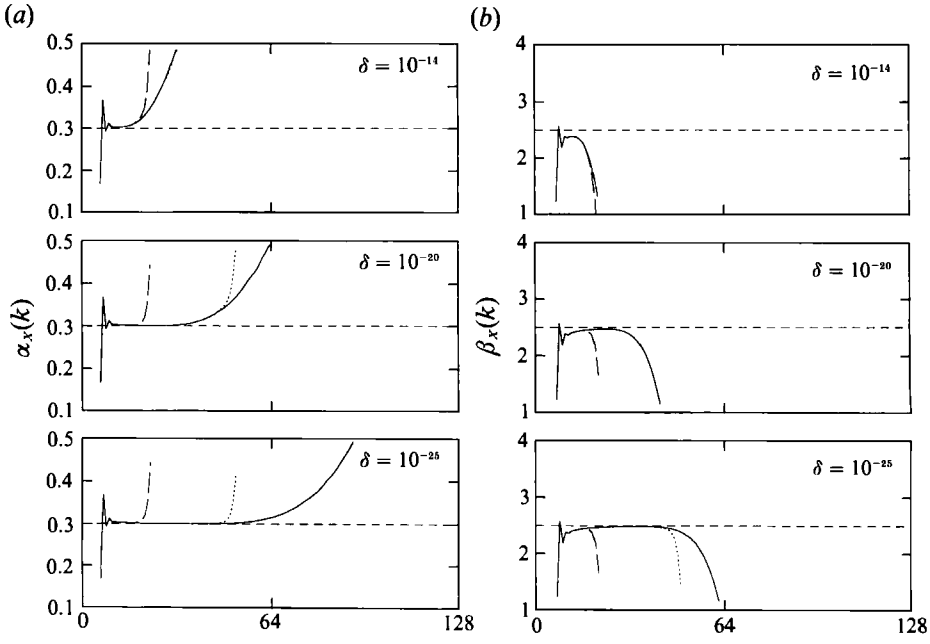

FIGURE 7. (*a*) The fit to $\alpha_X(k)$ at $t = 1.4$ for different values of N and δ, for $a = \frac{1}{2}$. Each box shows the fit for a fixed value of δ (10^{-14}, 10^{-20} and 10^{-25}), $N =$ ————, 64; – – –, 128 and ——, 256. The horizontal dashed line is at 0.30. (*b*) The fit to $\beta_X(k)$ at $t = 1.4$ for different values of N and δ, as in (*a*). The dashed line is at $\frac{5}{2}$.

through the asymptotic decay of the Fourier spectrum. Figure 7(*a*) shows the influence of both N and δ upon the fit to $\alpha_X(k)$ at $t = 1.4$, for $a = 0.5$. In each box, δ is kept fixed, and N is varied ($N = 64$ (solid–dashed), 128 (dot–dot), and 256 (solid)). The dashed line is at what seems to be the k-independent value of α_X from the fit (0.30). Consider the top box, for which $\delta = 10^{-14}$ and $K_\delta \approx 65$. It appears that as N is increased, the fits to $\alpha_X(k)$ collapse onto a limiting curve, which if the above argument is valid, should be obtained for those fits in which $K_\delta \leqslant \frac{1}{2}N$. This is the case for both $N = 128$ and 256, for which the fits lie upon one another. Now, examining the other two boxes for which $\delta = 10^{-20}$ and $\delta = 10^{-25}$, it is clear that the limiting behaviour is strongly dependent upon δ, and that as δ is decreased the limiting curve has a broader and broader range of k-independent values. This same behaviour is even more pronounced in the fit to β_X, shown in figure 7(*b*). Here the dashed line is at $\frac{5}{2}$, the k-independent value of $\beta_X(k)$ suggested by Moore's analysis. As in figure 7(*a*), as N is increased, and δ decreased, $\beta_X(k)$ evinces a broader and broader range of k-independent behaviour, and apparently asymptotes to $\frac{5}{2}$. Similar behaviour is observed in the fits to $\alpha_Y(k)$ and $\beta_Y(k)$.

If the behaviour observed in figure 7(*a*, *b*) persists as N becomes larger and δ smaller, then it provides a very strong validation of Moore's analysis for the intermediate time behaviour of the vortex sheet. It is also clear that the higher precision was necessary to convincingly demonstrate that the spectrum behaves asymptotically as in (4.2). A similar analysis will be performed (again, for $a = \frac{1}{2}$) very near the singularity time.

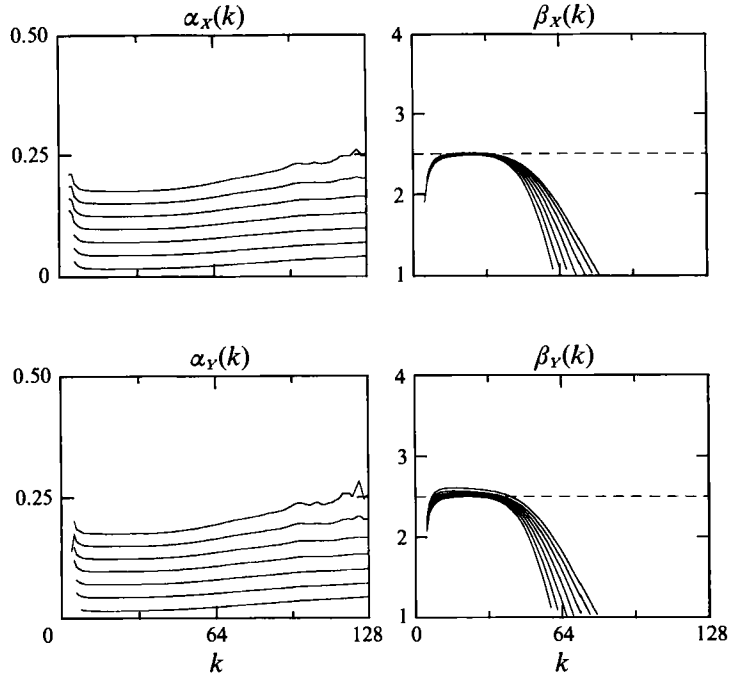

FIGURE 8. The fits to α_X, β_X, α_Y and β_Y using Ansatz (4.4), for $a = \frac{1}{8}$, from $t = 2.85$ to 3.0 at intervals of 0.025. The dashed line is at $\frac{5}{2}$.

4.2. *Vortex sheet behaviour near the singularity time*

We now turn to the behaviour of the vortex sheet near its singularity time, again considering first the smallest-amplitude case, $a = 0.125$. Recall from §4.1 that Moore's analysis predicts $t_c \approx 2.84$, while the numerical results suggest that the solution is still analytic at $t = 2.85$. From the numerical results we predict the true singularity to be $t_c \approx 3.015$, and now consider the evolution up to $t = 3.0$.

The results given here have $N = 512$, $\Delta t = 0.005$, and $\delta = 10^{-25}$. It was too costly to perform such a high resolution calculation from $t = 0$, so the following method was used: an initial condition, for the MPVA with $N = 512$, was generated by doubling the $N = 256$ data at $t = 2.55$ through the discrete Fourier transform. Doubling in this way gave some improvement in the results near the critical time, when $K_\delta \gg \frac{1}{2}N$. However, doubling the number of points again, to 1024, at $t = 2.85$, using the same criteria and method as above, led to no change in the results, suggesting an error dominated by the value of δ, not of N. Again, the Hamiltonian is conserved to at least ten digits throughout the calculation.

Figure 8 shows the fits to α_X, β_X, α_Y and β_Y, using Ansatz (4.4) for $a = 0.125$, from $t = 2.85$ to 3.0 at intervals of 0.025. From the fits to α_X and α_Y it is apparent that the motion of the sheet is becoming increasingly difficult to resolve. For sufficiently small k, say $k \leqslant 64$, the fits are still quite flat, but show a slight positive slope for larger k. Nonetheless, the values of α_X and α_Y show a general decrease towards zero as time increases, and again coincide in value. Over the range where all α are flat, β_X is again fit well by $\frac{5}{2}$, shown as a dashed line in the graph. On the other hand, the fit to β_Y shows a divergence away from $\frac{5}{2}$ to some larger value. Choosing $k = 23$ as representative, figure 9 shows the fits to α_Y and β_Y as functions of time. The trend of α_Y towards zero is clear. Extrapolations to zero give the previously stated estimate

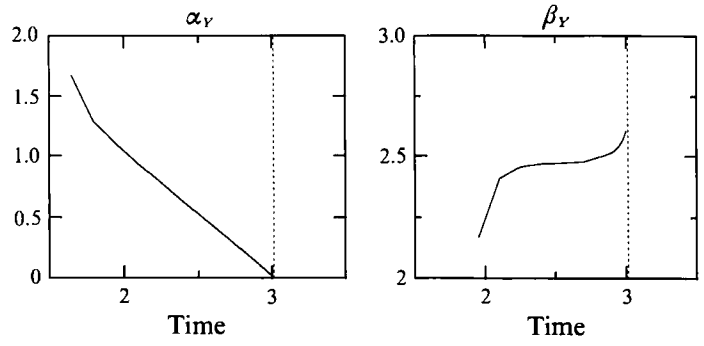

FIGURE 9. The evolution of α_Y and β_Y at $k = 23$, for $a = \frac{1}{8}$. The dashed line is at the estimated singularity time of 3.015.

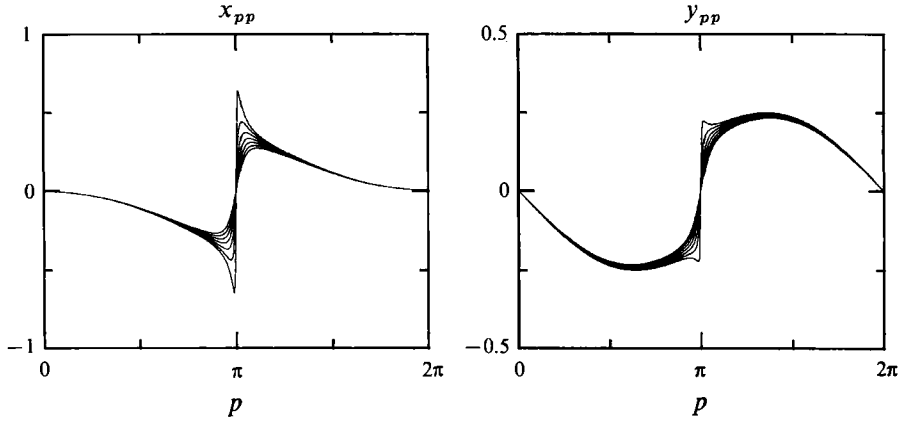

FIGURE 10. The evolution of $x_{pp}(p,t)$ and $y_{pp}(p,t)$, for $a = \frac{1}{8}$, at the same times as in figure 8.

of the critical time as $t_c \approx 3.015 \pm 0.005$. The fit to β_Y shows a range in time over which the fit is close to $\frac{5}{2}$, but as the singularity time is approached, an increase in its value is observed. By extrapolation we have that $\beta_Y \approx 2.6$ at the singularity time. This implies a slightly weaker divergence in $y(p,t_c)$ than Moore's analysis predicts, though in any case both $x_{pp}(p,t)$ and $y_{pp}(p,t)$ diverge as the critical time is approached. Figure 10 shows $x_{pp}(p,t)$ and $y_{pp}(p,t)$, at the same times as figure 8. The behaviour here is consistent with the difference in the estimated values of β_X and β_Y at $t = t_c$; $x_{pp}(p,t)$ is diverging more quickly than $y_{pp}(p,t)$ as the singularity time is approached.

A similar behaviour is observed for evolution of the sheet with $a = 0.25$. In this case, the extrapolated value of β_Y is approximately 2.7, rather than 2.6, again giving a slightly weaker divergence in y_{pp} than Moore's analysis predicts. A more pronounced difference in behaviour is seen at larger values of a, where y_{pp} can apparently remain bounded at the singularity time.

We examine now the behaviour of the vortex sheet near its singularity time for the case $a = 0.50$. The results given here have $N = 512$ with $\Delta t = 0.0025$, and $N = 1024$ with $\Delta t = 0.001\,25$. In both cases, $\delta = 10^{-25}$. Here the number of computational points are first doubled from the $N = 256$ data at $t = 1.3$, and then again at $t = 1.5$ using the same criteria and method as discussed above. The singularity time is estimated to be $t_c \approx 1.615$. The $N = 512$ results are shown up to $t = 1.6$. The

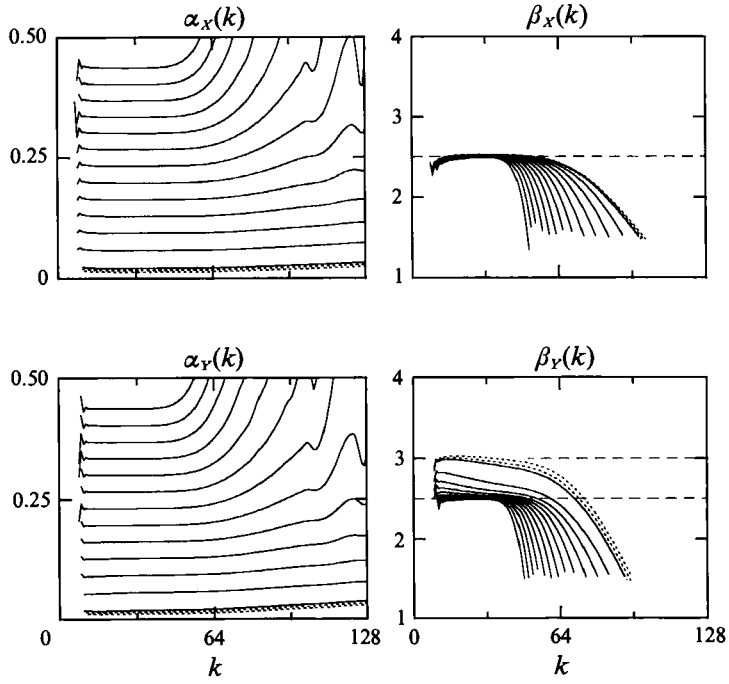

FIGURE 11. The fits to α_X, β_X, α_Y and β_Y using Ansatz (4.4), for $a = \frac{1}{2}$. ———, $t = 1.4$ to 1.6 at intervals of 0.025, and are fit from $N = 512$ data. – – –, $t = 1.6$, 1.6025 and 1.605, are fit from $N = 1024$ data. The dashed horizontal lines are at $\frac{5}{2}$ and 3.

resolution study presented in the next subsection indicates the computed solution with $N = 512$ has at least five significant digits of accuracy at this time. By $t = 1.605$, the width of the strip of analyticity is almost half of that at $t = 1.6$. It is from $t = 1.6$ to $t = 1.605$ that the $N = 1024$ data is shown. However, as with the $a = \frac{1}{8}$ case, increasing the number of points to $N = 1024$ does not yield further increases in the range over which the fits appear to be correct. This suggests an error that is dominated by the size of δ rather than of N. Again, the Hamiltonian is conserved to at least ten digits throughout the calculation, and further decreases in the timestep do not change the results.

Figure 11 shows the fits to α_X, β_X, α_Y and β_Y, using Ansatz (4.4). The solid curves are from $t = 1.4$ to $t = 1.6$, at intervals of 0.025, and are fit from the $N = 512$ data. Closer to the singularity time are the dashed curves, fit from the $N = 1024$ data, which are from $t = 1.60$ to 1.605 at intervals of 0.0025 (i.e. the $N = 512$ and $N = 1024$ results overlap at $t = 1.6$). A horizontal line at $\beta_Y = 3$ has been added to the lower right-hand figure.

The difference in behaviour of the fits for the algebraic decay is very apparent. β_X is still well fit by a value of $\frac{5}{2}$, which would yield a divergent second derivative. The fit to β_Y suggests a transition from an algebraic decay of $k^{-\frac{5}{2}}$ for $Y_k(t)$, to decay close to k^{-3}. That the transition begins at intermediate wavenumbers, then spreads upward to higher wavenumbers, is reminiscent of the behaviour observed by Sulem *et al.* (1983) in their study of singularity formation in the inviscid Burgers' equation. There, two square root singularities (from above and below, as in (2.13)) collide on the real axis to form a cube root singularity in the solution. The transition to a spectral decay associated with a cube root singularity begins at intermediate wavenumbers, and spreads upwards as the singularity time is approached. To have

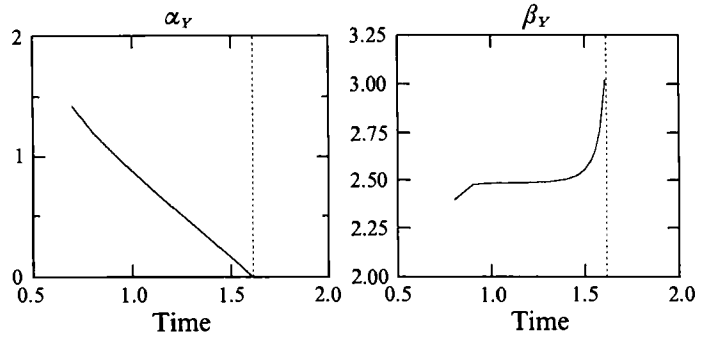

FIGURE 12. The evolution of α_Y and β_Y at $k = 23$, for $a = \frac{1}{2}$. The dashed line is at the estimated singularity time of 1.615.

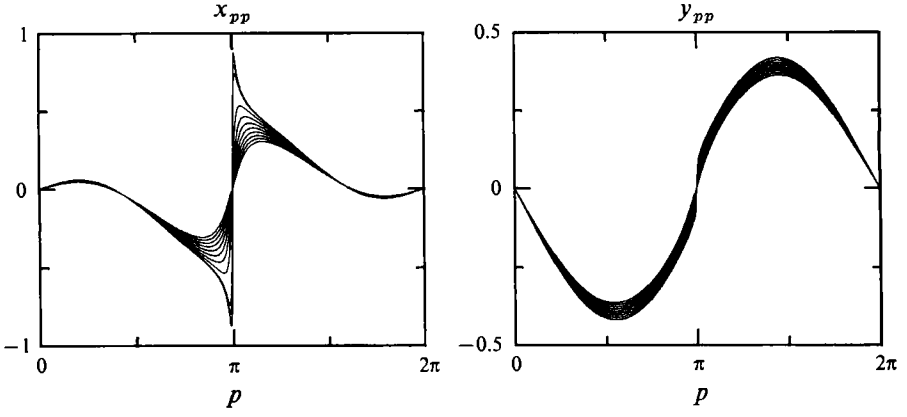

FIGURE 13. The evolution of $x_{pp}(p,t)$ and $y_{pp}(p,t)$, for $a = \frac{1}{2}$, at the same times as in figure 11.

precisely a k^{-3} decay at the singularity time would be consistent with $y_{pp}(p,t_c)$ having a step discontinuity, and remaining bounded. However, it appears that the fit to β_Y is rising above 3 as the singularity time is approached. Again choosing $k = 23$ as characteristic, figure 12 shows the fits to α_Y and β_Y as functions of time. Again, the decrease of α_Y towards zero is evident, and extrapolations to zero of α_X and α_Y give $t_c = 1.615 \pm 0.005$. The transition of β_Y from $\frac{5}{2}$ is also evident, and the fit to β_Y exceeds 3 near the singularity time. Extrapolations to the singularity time gives values of β_Y close to 3.1, suggesting that y_{pp} is both bounded and continuous near the singularity time. Figure 13 shows $x_{pp}(p,t)$ and $y_{pp}(p,t)$, at the same times as figure 11, though for the sake of clarity, the $N = 1024$ curves are solid rather than dashed. As is consistent with Moore's analysis and its apparent spectral decay (see figure 11), $x_{pp}(p,t)$ is diverging at $p = \pi$, in the form of an infinite jump discontinuity. However, in contrast to the smaller-amplitude cases, and in agreement with having a spectral decay of at least k^{-3} at the critical time, $y_{pp}(p,t)$ is not diverging, but remaining bounded as the singularity time is approached (its derivative $y_{ppp}(p,t)$ is becoming infinite as $t \to t_c$; extrapolations of $1/x_{ppp}(\pi,t)$ or $1/y_{ppp}(\pi,t)$ to zero gives estimates for the critical time very close to those obtained by extrapolations of α_X or α_Y to zero.)

The last case considered is with $a = 1.0$. Here the form of the singularity in $y(p,t)$ seems to have changed more profoundly. As with the smaller-amplitude initial data, the fits to β_X are well-matched by $\frac{5}{2}$, even up to the singularity time. The fits to α_X

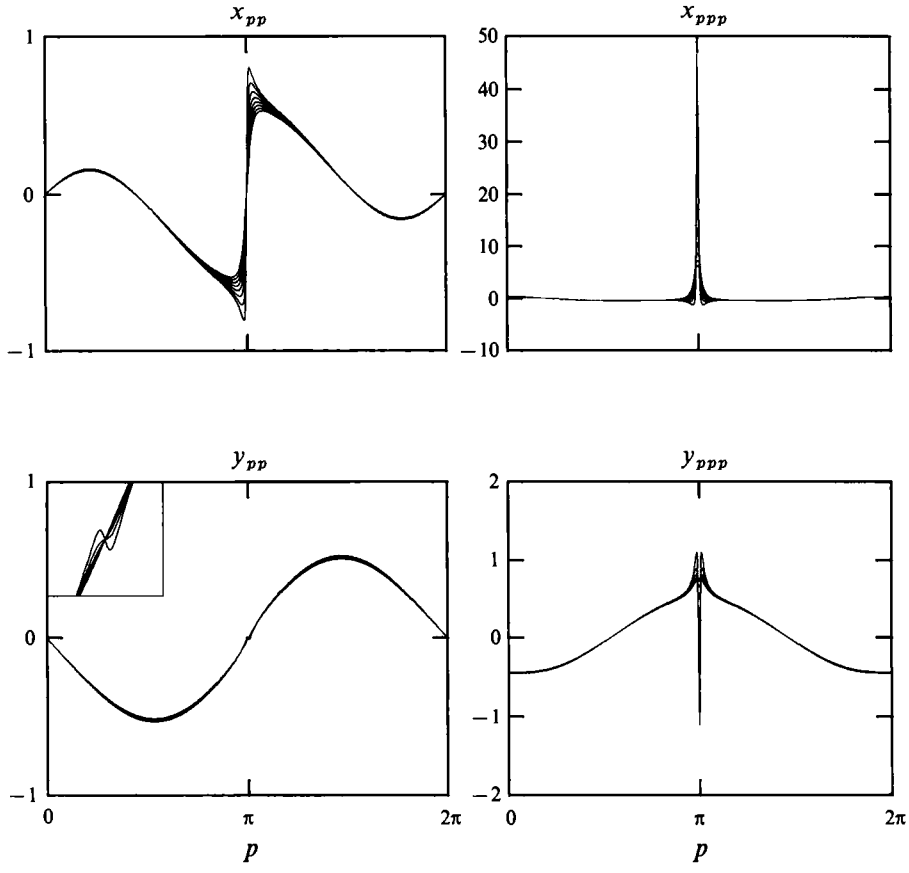

FIGURE 14. The evolution of $x_{pp}(p,t)$, $x_{ppp}(p,t)$, $y_{pp}(p,t)$ and $y_{ppp}(p,t)$ for $a = 1$, from $t = 1.025$ to 1.06875 at intervals of 0.00625. The inset in the lower left-hand box is an enlargement of $y_{pp}(p,t)$ about $p = \pi$.

are flat over a large range in k, and in time show a monotonic decrease to zero. Extrapolations of α_X to zero give $t_c \approx 1.10$. Again, at intermediate times, the fit β_Y is also well-matched by $\frac{5}{2}$, but then begins a transition away from $\frac{5}{2}$, apparently to larger values. However, as the singularity time is approached this fit becomes incoherent, and shows no uniform behaviour in β_Y. Figure 14 shows $x_{pp}(p,t)$, $x_{ppp}(p,t)$, $y_{pp}(p,t)$ and $y_{ppp}(p,t)$ from $t = 1.025$ to 1.06875 at intervals of 0.00625. An enlargement of y_{pp} about $p = \pi$ is included in the upper left-hand corner. For the times shown, $N = 1025$, $\delta = 10^{-25}$ and $\Delta t = 0.00125$ (the usual doublings of the $N = 256$ data have been performed).

The behaviour of x_{pp} (and x_{ppp}) is similar to that of x_{pp} for smaller values of a as their singularity times are approached (for example, see the left-hand boxes in figures 10 and 13). Also for the smaller values of a, both x_{ppp} and y_{ppp} grow and diverge positively at a single maximum at $p = \pi$. This behaviour has now changed. For the first three times shown, y_{ppp} has a single positive maximum at $p = \pi$. This maximum then bifurcates into two nearby, local maxima, and the newly created minimum between them decreases rapidly in value. The formation of the negative extrema at $p = \pi$ is reflected in the small structure which develops in y_{pp} (magnified in the inset). This change in behaviour may explain the breakdown of the Ansatz in this instance. The choice of the Ansatz for the large k behaviour of the spectrum ($Y_k \approx Ak^{-\beta}e^{-\alpha k}$)

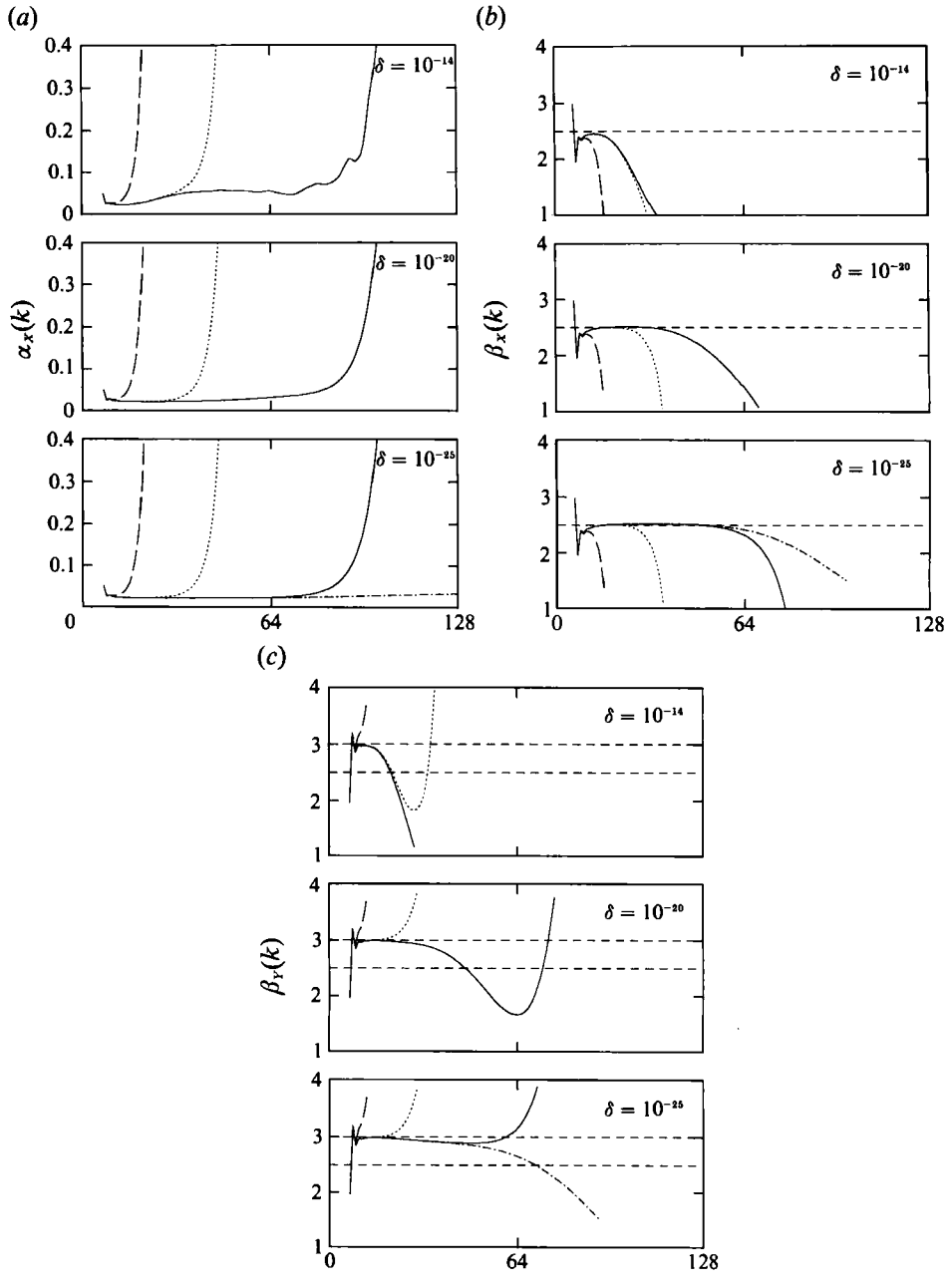

FIGURE 15. (*a*) The fit to $\alpha_X(k)$ at $t = 1.6$ for different values of N and δ, for $a = \frac{1}{2}$. Each box shows the fit for a fixed value of δ (10^{-14}, 10^{-20} and 10^{-25}), as $N =$ ———, 64; – – –, 128; ——, 256; —·—, 512 (bottom box only). (*b*) The fit to $\beta_X(k)$ at $t = 1.6$ for different values of N and δ, as in (*a*). The dashed line is at $\frac{5}{2}$. (*c*) The fit to $\beta_Y(k)$ at $t = 1.6$ for different values of N and δ, as in (*a*). The dashed lines are at $\frac{5}{2}$ and 3.

is predicated upon very specific assumptions on the type and location of singularities in the complex extension of the solution. Namely, it is assumed that above (and likewise below) the real axis, there is but one singularity closest to the real axis, and that it is of branch type (see 2.13). It seems likely that one of these assumptions has

broken down, and that the incipient singularity structure is not well described by (4.4). However, we are unable to supply a definitive cause. Further, we found it difficult to resolve this structure further towards the singularity time reliably, but we do note that the observed behaviour has persisted under changes in resolution.

4.3. *The dependence upon numerical parameters near the singularity time*

At $t = 1.6$, immediately before the posited singularity time for $a = 0.50$, the effect upon the results of varying both N and δ is examined. An assessment of the errors of the calculations is also made.

Using Ansatz (4.4), figures 15(*a*), 15(*b*) and 15(*c*) show $\alpha_X(k)$, $\beta_X(k)$, and $\beta_Y(k)$, respectively, for the same values of N and δ as in figures 7(*a*) and 7(*b*), with the addition of the fits to the data with $N = 512$ and $\delta = 10^{-25}$ (the dot–dash curve in the lower box). Recall that this calculation was started from $t = 1.3$, at which time $K_\delta < \frac{1}{2}N$, by doubling the data with $N = 256$. The results for $\alpha_Y(k)$ are similar to those for $\alpha_X(k)$ and are not shown. At this time, even though $K_\delta \gg \frac{1}{2}N$ for all the various cases shown, the value of the cutoff δ plays a large role in behaviour of the fits. This influence is perhaps least seen in the behaviour of α_X, which governs the dominant (albeit vanishing) exponential decay of the spectrum. The fits with $N = 64$ and 128 show relatively little change as δ is decreased. For $N = 256$, decreases in δ give additional smoothness and flattening of the fit. As figure 15(*b*) shows, fits to determine the algebraic part of the spectral decay are much more sensitive. Indeed, it is only for $N = 64$ that the fits are independent of δ, and these fits are poor at best. For $\delta = 10^{-14}$ (the upper box), the fits at both larger values of N are dominated by the size of δ. The $N = 128$ fit has assumed its δ independent form with $\delta = 10^{-20}$, and the $N = 256$ fit perhaps only with $\delta = 10^{-25}$. It seems typical of a fit, at a particular value of N, to decrease more rapidly away from $\frac{5}{2}$ as the fit loses its dependence upon δ. For example, the fit with $N = 256$ has a larger second derivative as it falls away from $\frac{5}{2}$ with $\delta = 10^{-25}$, than at the two larger values of δ. By this somewhat subjective standard, it appears that the fit with $N = 513$ and $\delta = 10^{-25}$ has not yet reached a form independent of δ. This is evident as well in the fits for β_Y in figure 15(*c*), where the increase to $N = 512$ at $\delta = 10^{-25}$ gives little apparent increase in asymptotic behaviour. Nonetheless, the fits to determine the algebraic part of the decay generally seem to converge to some asymptotic form as N is increased and δ is decreased. For β_X this is a value of $\frac{5}{2}$, in accordance with Moore's theory, while for β_Y the asymptotic form is related to a transition in the spectral decay away from $k^{-\frac{5}{2}}$.

Through figure 16 an assessment is made of the errors in the calculations for $a = \frac{1}{2}$. Only the calculations with $\delta = 10^{-25}$ are considered. Neglecting time-discretization errors and assuming that the MPVA is a convergent approximation, an estimate for the spatial error in z_j^N (the superscript denotes the number of points in the spatial discretization) is given by

$$L_\infty^{mN,N} = \max_{0 \leqslant j \leqslant N-1} |z_{mj}^{mN}(t) - z_j^N(t)|. \tag{4.5}$$

For $m > 1$, $L_\infty^{mN,N}$ measures the maximum difference between the two computed discrete solutions, z^{mN} (with mN points) and z^N (with N points), at their N common values under the discretization of p.

In figure 16, the negative logarithm of this quantity is plotted. In the left-hand box, the dashed curves are for $L_\infty^{256,64}$ and $L_\infty^{256,128}$ for $0 \leqslant t \leqslant 1.65$, and the solid curves are $L_\infty^{512,64}$, $L_\infty^{512,128}$, and $L_\infty^{512,256}$ on $1.3 \leqslant t \leqslant 1.65$. Again, the $N = 512$ calculation was that started at $t = 1.3$ by doubling the $N = 256$ data. The $N = 128$

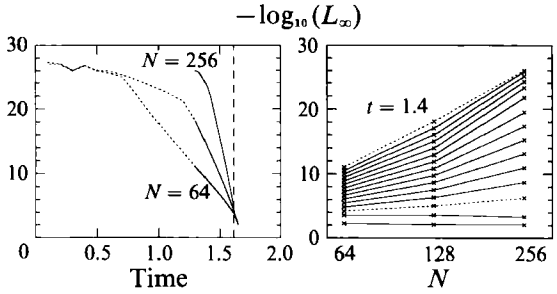

FIGURE 16. The left-hand box shows ---, $-\log_{10}(L_\infty^{256,N})$ from $t = 0$ to 1.65 for $N = 64$ and 128, and ——, $-\log_{10}(L_\infty^{512,N})$ from $t = 1.4$ to 1.65, for $N = 64$, 128 and 256. The dashed vertical line is at $t = 1.615$. The right-hand box shows $-\log_{10}(L_\infty^{512,N})$ as a function of N on a horizontal logarithmic scale, from $t = 1.4$ to 1.65 at intervals of 0.025. The short-dashed curves are with $t = 1.4$ and 1.6.

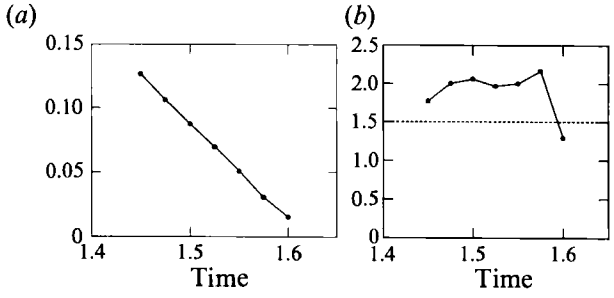

FIGURE 17. The error in the right-hand box of figure 16 is fit with the form $E \approx A\,\mathrm{e}^{-aN}/N^q$ at times near the singularity time. (*a*) The value of a in the fit; (*b*) the value of q. ---, $q = \frac{3}{2}$.

error is that lying above and below the $N = 64$ and $N = 256$ errors, respectively. The evidence is certainly that the method is converging in N up to the singularity time (shown as a vertical long-dashed line). Note that each of the three curves decays as the singularity time is approached. This is consistent with the error bound given in (3.5), in which the decay rate in the exponential error scales linearly with an analyticity strip width. The fits to α_X and α_Y suggest that the collapse of the analyticity strip width is nearly linear.

The right-hand box shows $L_\infty^{512,N}$ (again under the negative logarithm) on a horizontal logarithmic scale for $N = 64$, 128 and 256, from $t = 1.3$ to 1.65 at intervals of 0.25. The dashed curves are for $t = 1.3$ and $t = 1.6$. Faster than exponential convergence is suggested as these error curves have both positive slope and upward curvature as N is increased, up to and including $t = 1.6$. The lack of curvature of the topmost curves occurs because the errors for $N = 256$ are at the level of the Fourier filter (10^{-25}). Note that for $t = 1.625$ and 1.650, the slope of the error curve is negative, implying again that convergence is lost for this method beyond the singularity time.

The error bound given in (3.5) is only an upper bound. An optimal error estimate might be expected to have the form $E \approx A\,\mathrm{e}^{-aN}/N^q$ for large N. Figure 17 shows the fits for a and q using the three errors in the right-hand box of figure 16, for times close to the singularity time. The values of a agree very roughly with half the analyticity strip width, as estimated from the spectrum. This is consistent with the MPVA using only half of the points to evaluate the Birkhoff–Rott integral. The positive values for q demonstrate the faster than exponential convergence. As remarked in §3, the MPVA has an error of $O(1/N^{\frac{1}{2}})$ to the Birkhoff–Rott integral at the singularity time

for the singularity posited by Moore. As the Moore singularity appears to be the dominant one in this case, and the position is one order smoother than the velocity, we might expect to find $q = \frac{3}{2}$ in the position error (at least at the singularity time). The fitted values for q are actually closer to 2, except at the last time $t = 1.6$ for which we have $q \approx 1.3$. This suggests that even at the singularity time (though presumably not beyond), the MPVA is convergent to the sheet motion. As with the fits to the spectrum, higher-order terms may need to be included in the fit to get better estimates for these values. In any case, the positive values for a and q near the singularity time verify the convergence of the method.

Near the singularity time, the maximum error always occurs very close to $p = \pi$, the location of the nascent singularity. The maximum error cannot occur precisely at $p = \pi$ as this point is a fixed point of both the continuous and discrete flows. At $t = 1.6$ the maximum error of the $N = 256$ data from the $N = 512$ data occurs at $j = 129$, or one grid point to the right of $p = \pi$. The value of this error is 5.0×10^{-7}, and the two calculations ($N = 256$ and 512) agree to five significant digits. Given the apparent convergence at this time, the error for the $N = 512$ calculation is presumably less. If we use the values of a and q from figure 17 to estimate this error, we find as its value 3.7×10^{-9}.

All of the calculations discussed in this section used a fourth-order, Adams–Moulton, predictor–corrector method with a timestep of $\Delta t = 0.0025$. All indications are that the results are well-resolved in time. For example, halving the timestep for the $N = 512$ calculations from $t = 1.3$ gave a maximum difference between the two calculations of 1.2×10^{-8} at $t = 1.6$, and introduced no change in the results. The results reported here are also seen using the formulation (3.7) of the Birkhoff–Rott equation together with the alternate point quadrature. Additionally, the point-vortex approximation (PVA) has been implemented, and again consistent results are seen. The PVA calculations also showed a clear $O(1/N)$ convergence to the MPVA results near the singularity time (again $t = 1.6$).

4.4. *Further considerations*

While there are important differences between analytic prediction and numerical results, the general mechanism by which a planar vortex sheet becomes singular does not change. About a point along the sheet there is a rapid compression of the Lagrangian marker particles along the sheet. This compression is measured by $\hat{\gamma}(p,t)$, the true vortex-sheet strength, which is defined by

$$\hat{\gamma}(p,t) = \frac{\gamma(p)}{s_p(p,t)}, \tag{4.6}$$

where $s_p = (x_p^2 + y_p^2)^{\frac{1}{2}}$. s_p is the derivative of arclength with respect to the Lagrangian variable p, and is an infinitesimal measure of the distance between Lagrangian points on the sheet. Thus, as the particles become compressed along the sheet about some point, the value of s_p decreases there, and $\hat{\gamma}$ increases. Recall that $\hat{\gamma}$ gives the jump in tangential velocity across the sheet. It is because the vorticity must remain confined to the sheet and does not have degrees of freedom of smoother vorticity distributions, which can bulge outwards and form a vortex (Baker & Shelley 1990), that this compression leads to the formation of singularities. This is illustrated in figure 18, which shows $\hat{\gamma}$ as a function of the signed arclength of the sheet from $p = \pi$, from $t = 1.3$ to $t = 1.6$ at intervals of 0.05, for the case $a = 0.5$. $\hat{\gamma}$ is given initially by $\gamma(p, t = 0) = -p + \frac{1}{2}\cos(p)$ (dashed). Around the local extremum at $p = \pi\,(s = 0)$, $\hat{\gamma}(p,t)$ becomes concentrated, and increasing in amplitude. There is a corresponding

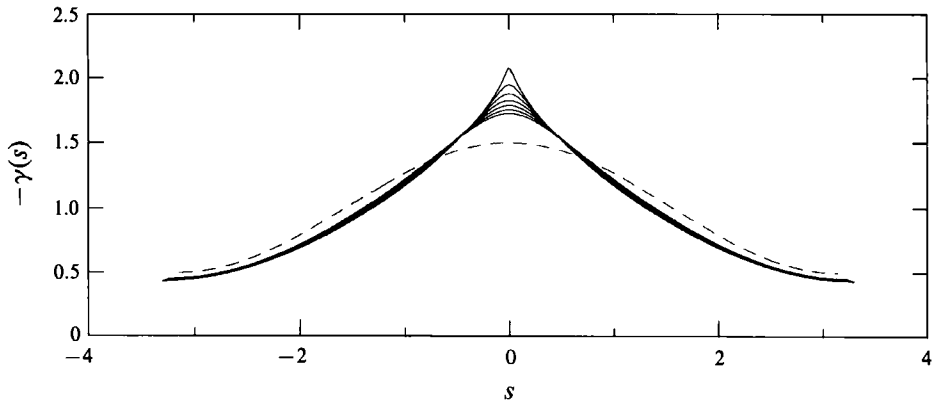

FIGURE 18. The evolution of $\hat{\gamma}(s,t)$, for $a = \frac{1}{2}$, from $t = 1.3$ to 1.6 at intervals of 0.05, as a function of the signed arclength from $p = \pi$. Increasing amplitude corresponds to increasing time. The dashed curve is $\hat{\gamma}(s, t = 0)$.

decrease in its amplitude away from the centre, as the area beneath $\hat{\gamma}(s)$ over a period is the circulation and is a conserved quantity. Moore's analysis predicts that at $t = t_c$, $\hat{\gamma}(p,t)$ is finite, with a square-root cusp at $p = \pi$. As the singularity in $x(p,t)$ remains of the form predicted by Moore, and that in $y(p,t)$ only weakens, this conclusion remains unchanged. From (4.6), the time rate-of-change of $\hat{\gamma}$ is given by

$$\frac{\mathrm{d}}{\mathrm{d}t}\hat{\gamma}(p,t) = -\hat{\gamma}(p,t)\,[\boldsymbol{s}(p,t)\cdot\boldsymbol{u}_s(p,t)],$$

or

$$\frac{\mathrm{d}}{\mathrm{d}t}\hat{\gamma}^2(p,t) = -2\hat{\gamma}^2(p,t)\,[\boldsymbol{s}(p,t)\cdot\boldsymbol{u}_s(p,t)], \tag{4.7}$$

where $\boldsymbol{s} = (x_p, y_p)/s_p$ is the unit tangent vector to the sheet, and $\boldsymbol{u}_s = (u_p, v_p)/s_p$ with $(u(p), v(p))$ the velocity of a Lagrangian particle on the sheet determined from (2.1). From (4.7), it is seen that $\hat{\gamma}(p,t)$ increases in magnitude only if $\boldsymbol{s}(p,t)\cdot\boldsymbol{u}_s(p,t) < 0$, or equivalently, if $\boldsymbol{s}$ and $\boldsymbol{u}_s$ are anti-aligned. Our results indicate that at the singularity time, $\boldsymbol{s}\cdot\boldsymbol{u}_s$ diverges as the inverse square root about $p = \pi$. More specifically, at $t = t_c$, $\boldsymbol{s}$ and s_p exist and are well-defined everywhere along the sheet, but u_p diverges as the inverse square root at $p = \pi$. Thus, at the singularity time, $\hat{\gamma}$ has finite value, but infinite temporal rate of change.

It can also be concluded that the velocities on and about the sheet remain bounded at the singularity time. In particular, the velocities immediately above and below the sheet at $p = \pi$, which is also a stagnation point of the sheet motion, can be given simply as

$$\boldsymbol{u}^{\pm}|_{p=\pi} = \tfrac{1}{2}\hat{\gamma}\boldsymbol{s},$$

and thus remain bounded. However, the strain rates in the fluid adjacent to the sheet do diverge. The conjugate velocity at a point η, not on the sheet, is given by

$$q^*|_\eta = (\boldsymbol{u} - \mathrm{i}v)|_\eta = \frac{1}{2\pi\mathrm{i}}\int_{-\infty}^{+\infty}\frac{\gamma(q)\,\mathrm{d}q}{\eta - z(q)}. \tag{4.8}$$

To calculate rates-of-strain, we need to find $\mathrm{d}q^*/\mathrm{d}\eta$ which can be given as

$$\frac{\mathrm{d}q^*}{\mathrm{d}\eta}(\eta) = \frac{1}{2\pi\mathrm{i}}\int_{-\infty}^{+\infty}\frac{\mathrm{d}}{\mathrm{d}q}\left[\frac{\gamma(q)}{z_q(q)}\right]\frac{\mathrm{d}q}{\eta - z(q)}. \tag{4.9}$$

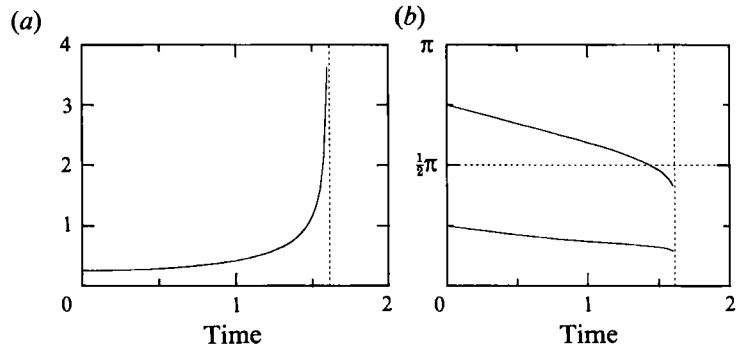

FIGURE 19. (*a*) The evolution of the extensional rate-of-strain at $p = \pi$ for $a = \frac{1}{2}$. ---, $t = 1.615$. (*b*) The evolution of the angle between the principal axis of compressional strain and the tangent vector to the sheet (lower curve), and the angle of the principal axis of extensional strain to the x-axis (upper graph). ---, $t = 1.615$, angle $= \frac{1}{2}\pi$.

This follows by exchanging derivatives with respect to η for derivatives with respect to q within the integral, and then performing an integration by parts. Letting $\eta \to z(p)^{\pm}$, i.e. from above and below, the Plemelj formula (Carrier *et al.* 1966, p. 414) yield

$$\left.\frac{\mathrm{d}q^*}{\mathrm{d}\eta}\right|_{\eta=z(p)^{\pm}} = \mp\frac{1}{2z_p(p)}\frac{\mathrm{d}}{\mathrm{d}p}\left[\frac{\gamma(p)}{z_p(p)}\right] + \frac{1}{2\pi\mathrm{i}}P\int_{-\infty}^{+\infty}\frac{\mathrm{d}}{\mathrm{d}q}\left[\frac{\gamma(q)}{z_q(q)}\right]\frac{\mathrm{d}q}{z(p)-z(q)}. \tag{4.10}$$

We now note that

$$\begin{aligned}\frac{\mathrm{d}q^*}{\mathrm{d}s}(p) &= \frac{1}{s_p}(u_p(p) - \mathrm{i}v_p(p)) \\ &= \frac{z_p(p)}{s_p(p)}\frac{1}{2\pi\mathrm{i}}P\int_{-\infty}^{+\infty}\frac{\mathrm{d}}{\mathrm{d}q}\left[\frac{\gamma(q)}{z_q(q)}\right]\frac{\mathrm{d}q}{z(p)-z(q)},\end{aligned} \tag{4.11}$$

or

$$\left.\frac{\mathrm{d}q^*}{\mathrm{d}\eta}\right|_{\eta=z(p)^{\pm}} = \mp\frac{1}{2z_p(p)}\frac{\mathrm{d}}{\mathrm{d}p}\left[\frac{\gamma(p)}{z_p(p)}\right] + \frac{s_p(p)}{z_p(p)}\frac{\mathrm{d}q^*}{\mathrm{d}s}(p). \tag{4.12}$$

In particular, at $p = \pi$, $\gamma(p)/z_p(p)$ is an even function, and the first term is zero, leaving

$$\left.\frac{\mathrm{d}q^*}{\mathrm{d}\eta}\right|_{\eta=z(\pi)^{\pm}} = \frac{s_p(\pi)}{z_p(\pi)}\frac{\mathrm{d}q^*}{\mathrm{d}s}(\pi). \tag{4.13}$$

Thus, at $p = \pi$, the straining flows above and below the sheet are equal. By our previous remarks, at least the real part of $\mathrm{d}q^*/\mathrm{d}s$ is diverging. This leads to the conclusion that the strain rates are also diverging. Also note that (4.11) allows the evolution of $\hat{\gamma}$ to be related to the local strain rates about the sheet, which are themselves determined globally.

It is of interest to examine the principal axes of strain at $p = \pi$, with their associated rates-of-strain, as calculated from (4.11) and (4.13). The integral in (4.11) can again be calculated by an alternate point quadrature rule, and by the same arguments, is again a spectrally accurate approximation so long as the solution $z(p, t)$ is analytic. Recall that the strain rates must add up to zero, and thus come as plus and minus pairs (extensional and compressional rates of strain, respectively), and that the associated principal axes of strain are orthogonal. Figure 19(*a*) shows the extensional (positive) rate-of-strain at $p = \pi$, for $a = 0.5$. It is clearly diverging as

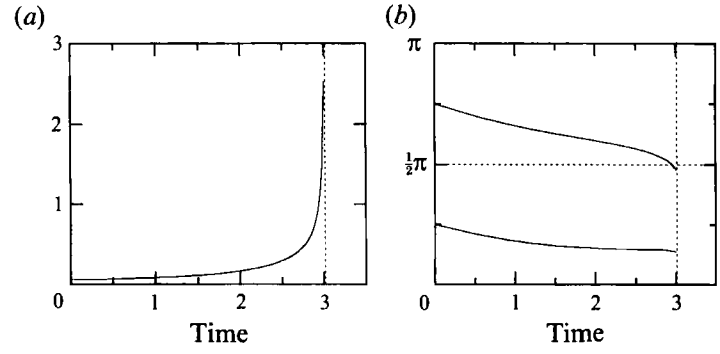

FIGURE 20. The same as figure 19, except that $a = \frac{1}{8}$, and the vertical lines are at $t = 3.015$.

$t \to t_c$, which is included as a dashed line in the figure. Figure 19(b) contains two graphs: the lower graph shows the angle between the principal axis of compressional rate-of-strain and the tangent vector to the sheet, at $p = \pi$. As the flow evolves, this angle decreases, implying increasing advection of vorticity towards this point. Coincident with this advection, the rate is also diverging, as shown in figure 19(a). The upper graph (figure 19(b)) shows the angle which the principal axis of extensional rate-of-strain axis makes with the x-axis. Near the singularity time, when the rates-of-strain are diverging, the direction of this axis overshoots an angle of $\frac{1}{2}\pi$, shown as a horizontal dashed line. This perhaps provides some explanation as to why the y-component of the solution is not diverging as quickly as the x. The singularity time, as calculated from the simulations, is again included as a dashed line. This behaviour is independent of amplitude, as seen in figure 20, which shows the same quantities, but for $a = 0.125$. Again, near the singularity time, the extensional rate-of-strain overshoots an angle of π at the singularity time, but by a lesser amount. This is consistent with the difference in singular behaviour for the two amplitudes studied here.

5. Concluding remarks

The purpose of this work was to examine the generality of Moore's analysis in describing vortex-sheet motion and its associated singularity formation. It demonstrated that Moore's analysis is valid under the assumptions of its derivation. For small-amplitude data at times away from the singularity time, Moore's analysis correctly described the form of the nascent singularity as two branch points of order $\frac{3}{2}$, symmetrically the real p-axis. This was done in detail for the MBO initial conditions. Calculations from the initial conditions considered by Kr (see 2.15)), for a particular value of ϵ, have shown also a similar correspondence to Moore's analysis. In addition, it appeared that Moore's analysis well-described the initial motions of sheets with large initial data. However, at least for the range of amplitudes considered here, Moore's analysis did not precisely give the actual form of the singularity. At the singularity time, the real and imaginary parts of the solution become differentiated in behaviour, which was not predicted. Again, the calculation from an initial condition used by Kr shows a similar, differentiated behaviour near the singularity time.

Some calculations have also been performed for the initial condition used originally by Moore for his asymptotic analysis (i.e. initial condition (2.8)). Setting $\epsilon = 2\pi\hat{\epsilon}$, we

have considered initial amplitudes from $\hat{\epsilon} = 0.01$ down to 0.000625, by successive halvings. Curiously, for each amplitude considered we have found two singularities, rather than one, forming in both x_{pp} and y_{pp}. The distance between them (in p) decreases as $\hat{\epsilon}$ decreases. Kr has similarly noted, for initial data (2.15), that if the initial amplitude were sufficiently large then two singularities would form on the sheet. Using consistent units, Kr found there were two singularities for $\hat{\epsilon} = 0.08$ while for $\hat{\epsilon} = 0.01$ there was only one. This is probably a similar phenomenon. Extrapolations to zero of the separation distance between the two observed singularities suggests that the two singularities will coalesce into one for some value of $\hat{\epsilon}$ between 0.00027 and 0.00035.

The differences with Moore's analysis at the singularity time is presumably due to its exclusion of higher-order corrections which have become important. G. Baker (private communication) has performed a version of Moore's analysis for the inviscid Burgers' equation

$$\frac{\partial u}{\partial t}(x,t) + u(x,t)\frac{\partial u}{\partial x}(x,t) = 0, \tag{5.1}$$

with initial condition

$$u_0(x) = \epsilon \sin x,$$

and periodic boundary conditions. The method of characteristics gives that at $t_c(\epsilon) = 1/(2\epsilon)$, the solution acquires a cube root singularity at $x = \pi$ of the form

$$u(x,t_c) = \epsilon 6^{\frac{1}{3}}(\pi - x)^{\frac{1}{3}} + \Psi, \tag{5.2}$$

where Ψ contains less singular terms. Singularity formation in this context can be interpreted as the symmetric approach of two square root branch points to the real x-axis. They collide at $x = \pi$ in such a way as to yield a cube root. Baker has found that Moore's analysis in this case correctly describes the initial approach and order of the branch points, but incorrectly predicts that the form of the singularity remains a square root, rather than the cube root. The failure of Moore's analysis can be directly attributed to higher-order terms dropped in the asymptotic analysis.

Moore's analysis of the Fourier series, leading to the estimate of its asymptotic decay in (2.11), actually arises as a second level of asymptotic approximation for solutions of the Birkhoff–Rott equation. In Moore (1979), Moore first obtained from (2.1) a simpler approximate equation, which he showed in Moore (1985) to be equivalent to a system of two nonlinear conservation laws. It was upon this system of conservation laws that the second asymptotic analysis was performed, and which led to (2.11). A simpler derivation of Moore's conservation equations is given in Caflisch & Orellana (1986). It is possible that Moore's equation will themselves correctly describe the form of the singularity at the singularity time, and that the fault in the analysis observed in this work lies with the terms discarded in the second level of asymptotic approximation.

In their study of the motion of thin layers of constant vorticity, Baker & Shelley (1990) established the relation between vortex sheets and asymptotically thin vortex layers. By assuming that the limit of a thin vortex layer of mean thickness $H \ll 1$ is a vortex sheet with true vortex-sheet strength $\hat{\gamma}$, their asymptotic analysis gives

$$\hat{\gamma} = -\frac{1}{H}T, \tag{5.3}$$

where T is the local thickness of the layer as measured along the normal to the vortex sheet. Here the total circulation on the period is normalized to -2π. This is the

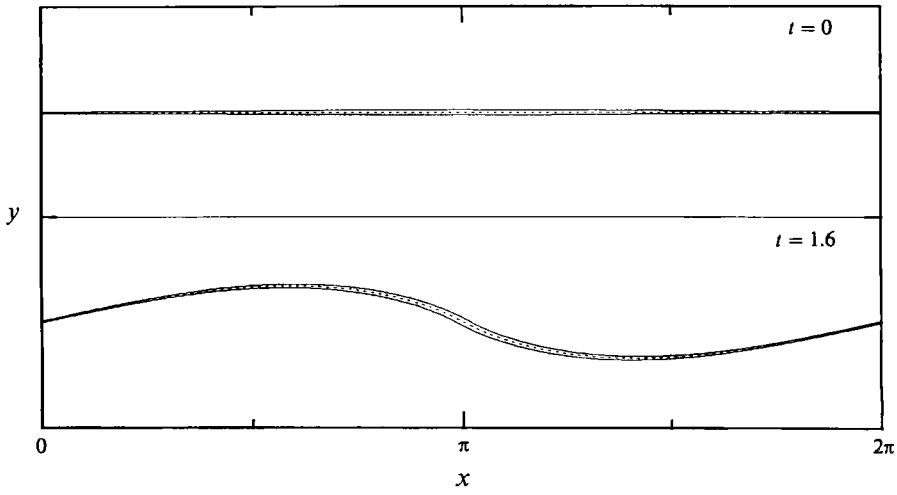

FIGURE 21. The boundaries of a layer of constant vorticity of mean thickness 0.025, which the vortex sheet models at $t = 0$ and $t = 1.6$, for $a = 0.5$, constructed from relation (5.3): ---, vortex-sheet positions.

intuitively appealing statement that $\hat{\gamma}$ is the product of the vorticity $(-1/H)$ and the local thickness T. This relation can be reversed; given a vortex sheet, what is the asymptotically thin vortex layer that it is modelling? Figure 21 shows the bounding profiles of a layer of constant vorticity, with $H = 0.025$, constructed using relation (5.3) from the vortex-sheet data with $a = 0.5$ at $t = 0$ (top box), and at $t = 1.6$ (bottom box). Recall that $t = 1.6$ is very nearly the singularity time for this case. The position of the vortex sheet is included as a dashed curve. Here the aspect ratio of the vortex layer is about 250:1. The figure shows that the initial perturbation in the vortex-sheet strength for the MBO initial conditions corresponds to a local thickening of the otherwise flat vortex layer. At $t = 1.6$, the concentration of $\hat{\gamma}$ about $p = \pi$ is reflected as a thinning of the layer away from the centre, and a further thickening in the centre. Simulations of vortex-layer motion from such initial conditions are also given in Baker & Shelley (1990), and show that after this point the vorticity reforms itself into a rotating elliptical core, with attached trailing arms. Such behaviour is apparently not accessible to solutions of the Birkhoff–Rott equation. However, the vortex sheet does provide an understanding of the initial straining flows that concentrate vorticity prior to their reforming into larger-scale vortex structures.

This work does not address the possible existence and nature of the vortex sheet after the singularity time, but has instead focused on gaining precise information on the form of the singularity. As has also been observed by Kr, no convergence of the numerical solution was observed after the singularity time. Of course, the spectral accuracy of the MPVA is lost in the present of singularities. At these later times, the motion becomes dominated by rigid scale interactions, and is apparently chaotic. It appears that mollification of some sort is necessary to study behaviour numerically past the singularity time (Krasny 1986*b*; Baker & Shelley 1990). Such studies indicate that the solution, if it exists, may have the form of doubly branched spiral. It is known that measured-valued solutions exist globally for vortex-sheet initial data, but the notion of such a solution is so general that it gives little information about its specific nature. The scaling of vorticity concentrations in the study of thin vortex layers by Baker & Shelley (1990) does not preclude the vortex sheet existing as a classical weak solution after the singularity time (Diperna & Majda 1987).

Explicit singular solutions have been constructed by Caflisch & Orellana (1989), with $\gamma(p) = 1$, which have the form

$$z(p,t) = p + s_0 + r,$$

where $$s_0 = \epsilon(1-\mathrm{i})\{[1-\exp(-\tfrac{1}{2}t-\mathrm{i}p)]^{1+\nu}-[1-\exp(-\tfrac{1}{2}t+\mathrm{i}p)]^{1+\nu}\},$$

ϵ is small, r is a correction term, and $\nu > 0$. $\nu = \frac{1}{2}$ would give the spatial structure of Moore's singularity at $t = 0$. The singularity found in this work is not of this form, though it is quite possible that such a singularity could be constructed analytically. Duchon & Robert (1988) have also constructed such explicit singular solutions.

Lastly, we end with a caveat. It is possible that Moore's asymptotic results are recovered only at yet smaller values of a than we have used here. Computing with very small values of a will require more computing resources and perhaps different methods. It appeared from the results that the smaller the value of a the less rapid the fit to the spectra became asymptotic in its behaviour. To access yet more of the spectrum with these methods, even more precise calculations will be necessary. It is also possible that such calculations would benefit from the use of a symplectic time integration method which would reflect the Hamiltonian structure of the modified point-vortex approximation.

I would like to thank P. Constantin, A. Majda, J. Lowengrub, D. Meiron, S. Orszag, V. Rom-Kedar, and most especially G. Baker and R. Caflisch, for useful discussions regarding this work. This work was partially supported under contracts ONR/DARPA N00014-86-K-0759 and ONR N00014-82-C-0451. Some of the computations were carried out on the Cray-XMP at Argonne National Laboratory. I am currently supported by a National Science Foundation Postdoctoral Research Fellowship.

REFERENCES

Baker, G. R., McCrory, R. L., Verdon, C. P. & Orszag, S. A. 1987 Rayleigh–Taylor instability of fluid layers. *J. Fluid Mech.* **178**, 161–175.

Baker, G. R., Meiron, D. I. & Orszag, A. A. 1980 Vortex simulations of the Rayleigh–Taylor instability. *Phys. Fluids* **23**, 1485–1496.

Baker, G. R., Meiron, D. I. & Orszag, S. A. 1982 Generalized vortex methods for free-surface flow problems. *J. Fluid Mech.* **123**, 477–501.

Baker, G. R. & Shelley, M. J. 1986 Boundary integral techniques for multi-connected domains. *J. Comput. Phys.* **64**, 112–132.

Baker, G. R. & Shelley, M. J. 1990 On the connection between thin vortex layers and vortex sheets. *J. Fluid Mech.* **215**, 161–194.

Birkhoff, G. 1962 Helmholtz and Taylor instability. *Proc. Symp. Appl. Math. Am. Math. Soc.* **13**, 55–76.

Birkhoff, G. & Fisher, J. 1959 Do vortex sheets roll up? *Circ. Mat. Palermo* **8**, 77–90.

Caflisch, R. & Lowengrub, J. 1989 Convergence of the vortex method for vortex sheets. *SIAM J. Numer. Anal.* **26**, 1060–1080.

Caflisch, R. & Orellana, O. 1986 Long time existence for a slightly perturbed vortex sheet. *Commun. Pure Appl. Maths.* **34**, 807–838.

Caflisch, R. & Orellana, O. 1989 Singular solutions and ill-posedness of the evolution of vortex sheets. *SIAM J. Math. Anal.* **20**, 293–307.

Carrier, G., Krook, M. & Pearson, C. 1966 *Functions of a Complex Variable.* McGraw-Hill.

Conte, R. 1979 Etude numerique des nappes tourbillonnaires. Thèse, DPh-G/PSRM, CEN. Saclay.

DUCHON, R. & ROBERT, R. 1988 Global vortex sheet solutions to Euler equations in the plane. *Commun. PDE* **13**, 215–224.

DIPERNA, R. & MAJDA, A. 1987 Concentrations in regularizations for 2-d incompressible flow. *Commun. Pure Appl. Maths.* **40**, 301–345.

EBIN, D. 1988 Ill-posedness of the Rayleigh–Taylor and Helmholtz problems for incompressible fluids. *Commun. PDE* **13**, 1265–1295.

KRASNY, R. 1986*a* A study of singularity formation in a vortex sheet by the point-vortex approximation. *J. Fluid Mech.* **167**, 65–93.

KRASNY, R. 1986*b* Desingularization of period vortex sheet roll-up. *J. Comput. Phys.* **65**, 292–313.

HOU, T., LOWENGRUB, J. & KRASNY, R. 1991 Convergence of a point vortex method for vortex sheets. *SIAM J. Numer. Anal.* **28**, 308–320.

LAMB, H. 1932 *Hydrodynamics*, 6th edn. Cambridge University Press.

LONGUETT-HIGGINS, M. S. & COKELET, E. D. 1976 *Proc. R. Soc. Lond.* A **350**, 1–26.

MCGRATH, F. J. 1967 Nonstationary plane flow of viscous and ideal fluids. *Arch. Rat. Mech. Anal.* **27**, 329–348.

MAJDA, A. 1987 Vortex dynamics: numerical analysis, scientific computing, and mathematical theory. In *Proc. of the First Intern. Conf. on Industrial and Applied Maths.* Paris.

MEIRON, D. I., BAKER, G. R. & ORSZAG, S. A. 1982 Analytic structure of vortex sheet dynamics. Part 1. Kelvin–Helmholtz instability. *J. Fluid Mech.* **114**, 283–298.

MOORE, D. W. 1979 The spontaneous appearance of a singularity in the shape of an evolving vortex sheet. *Proc. R. Soc. Lond.* A **365**, 105–119.

MOORE, D. W. 1985 Numerical and analytical aspects of Helmholtz instability. In *Theoretical and Applied Mechanics*, Proc. 16th IUTAM (eds F. I. Niordson & N. Olhoff), pp. 263–274.

PUGH, D. A. 1989 Development of vortex sheets in Boussinesq flows. PhD thesis, Imperial College, London.

ROSENHEAD, L. 1931 The formation of vortices from a surface of discontinuity. *Proc. R. Soc. Lond.* A **134**, 170–191.

SIDI, A. & ISRAELI, M. 1988 Quadrature methods for periodic singular and weakly singular Fredholm integral equations. *J. Sci. Comput.* **3**, 201–231.

SULEM, C., SULEM, P. L., BARDOS, C, & FRISCH, U. 1981 Finite time analyticity for the two and three dimensional Kelvin–Helmholtz instability. *Commun. math. Phys.* **80**, 485–516.

SULEM, C., SULEM, P. L. & FRISCH, H. 1983 Tracing complex singularities with spectral methods. *J. Comput. Phys.* **50**, 138–161.

VAN DER VOOREN, A. I. 1980 A numerical investigation of the rolling up of vortex sheets. *Proc. R. Soc. Lond.* A **373**, 67–91.

VAN DYKE, M. 1975 *Perturbation Methods in Fluid Mechanics.* The Parabolic Press.